

*Antti Kemppainen*

LIMITING PHENOMENA  
RELATED TO THE USE OF  
IRON ORE PELLETS IN A  
BLAST FURNACE

UNIVERSITY OF OULU GRADUATE SCHOOL;  
UNIVERSITY OF OULU,  
FACULTY OF TECHNOLOGY





ACTA UNIVERSITATIS OULUENSIS  
C Technica 546

*ANTTI KEMPPAINEN*

**LIMITING PHENOMENA RELATED  
TO THE USE OF IRON ORE PELLETS  
IN A BLAST FURNACE**

Academic dissertation to be presented with the assent of the Doctoral Training Committee of Technology and Natural Sciences of the University of Oulu for public defence in the OP auditorium (L10), Linnanmaa, on 13 November 2015, at 12 noon

UNIVERSITY OF OULU, OULU 2015

Copyright © 2015  
Acta Univ. Oul. C 546, 2015

Supervised by  
Professor Timo Fabritius  
Doctor Timo Paananen

Reviewed by  
Associate Professor Alexander Babich  
Docent Lena Sundqvist-Öqvist

Opponent  
Professor Henrik Saxén

ISBN 978-952-62-0953-1 (Paperback)  
ISBN 978-952-62-0954-8 (PDF)

ISSN 0355-3213 (Printed)  
ISSN 1796-2226 (Online)

Cover Design  
Raimo Ahonen

JUVENES PRINT  
TAMPERE 2015

## **Kemppainen, Antti, Limiting phenomena related to the use of iron ore pellets in a blast furnace.**

University of Oulu Graduate School; University of Oulu, Faculty of Technology

*Acta Univ. Oul. C 546, 2015*

University of Oulu, P.O. Box 8000, FI-90014 University of Oulu, Finland

### ***Abstract***

Most of the iron in the world is produced using a blast furnace process, which has iron ore (iron oxides) and coke as its raw materials. When pellets are used in a blast furnace, the iron burden material is charged in the form of pellets and fine, iron-rich by-products are charged typically in the form of cold-bonded briquettes at the top of the blast furnace. Coke is the primary fuel and reductant in the blast furnace. Coke reacts with the oxygen of the blast air and forms carbon monoxide in the up-flowing gas, which reduces the descending iron oxide burden. In addition, carbon and hydrogen bearing reductants are injected from the tuyeres in the lower part of the furnace. Hydrogen partially replaces the carbon monoxide as a reducing agent and changes the composition of the reducing gas. The high temperature properties of the burden have a significant effect on the flow of reducing gas and formation of the cohesive zone which markedly affect the furnace efficiency. The raw materials are commonly stored outdoors and therefore include moisture in varying amounts. In addition, the briquette contains chemically bound water.

The rate of injected reductants, the high temperature properties and the water content of the raw materials have significant effects on blast furnace performance. They cause various phenomena in the blast furnace which set limitations on the process. The limiting phenomena related to the use of pellets in the blast furnace were studied in this doctoral thesis with the aim of obtaining additional knowledge about the limiting phenomena.

The results show that hydrogen increases the reduction rate of iron oxides at temperatures below 850 °C. High water vapour concentration causes a rapid conversion through a catalysed water-gas shift reaction at above 300 °C in a gas mixture similar to the one in the upper part of the blast furnace. The reduction rate of the cold-bonded briquette is higher than pellets due to a self-reducing effect. The phase transformations occurring in the briquette during reduction follow the path of phase equilibria. The softening of the pellet is caused by the formation of melt which initiates wüstite dissolution in the surrounding slag phase.

**Keywords:** blast furnace, cold-bonded briquette, high temperature properties, injected reductant, iron ore pellet, moisture, reduction, softening



## **Kemppainen, Antti, Rautamalmipellettien käyttöön liittyvät rajoittavat ilmiöt masuunissa.**

Oulun yliopiston tutkijakoulu; Oulun yliopisto, Teknillinen tiedekunta

*Acta Univ. Oul. C 546, 2015*

Oulun yliopisto, PL 8000, 90014 Oulun yliopisto

### ***Tiivistelmä***

Suurin osa maailmassa valmistettavasta raudasta tuotetaan masuuniprosessilla, jonka pääraaka-aineita ovat rautarikaste eli raudan oksidit ja koksi. Masuunissa, jossa käytetään pellettiä, rautarikaste panostetaan pelletin muodossa ja hienojakeiset rautapitoiset sivutuotteet tyypillisesti kylmäsidottuna brikettinä masuunin huipulta. Koksi on masuunin pääasiallinen polttoaine ja pelkistin, joka masuunin sisään puhallettavan ilman hapen kanssa reagoidessaan muodostaa ylöspäin virtaavaan kaasuun hiilimonoksidia, joka pelkistää masuunin kuilussa vajoavat rautaoksidit. Lisäksi yleensä käytetään hiiltä ja vetyä sisältäviä pelkistysaineita, jotka injektoidaan masuuniin alaosan horneilta. Vety korvaa osittain hiilimonoksidia rautaoksidien pelkistimenä ja muuttaa pelkistävän kaasun koostumusta. Panosmateriaalien korkealämpötilaominaisuudet vaikuttavat suuresti kuilun kaasuvirtauksiin ja koheesiovyöhykkeen muodostumiseen masuunissa, mitkä vaikuttavat merkittävästi masuunin tehokkuuteen. Suurista määristä johtuen raaka-aineet varastoidaan usein ulkona, joten ne sisältävät kosteutta vaihtelevissa määrin. Lisäksi briketti sisältää kemiallisesti sitoutunutta vettä.

Injektoitavien pelkistysaineiden käyttömäärällä, raaka-aineiden korkealämpötilaominaisuuksilla ja vesipitoisuudella on merkittäviä vaikutuksia masuunin toimintaan. Ne aikaansaavat masuunissa erilaisia ilmiöitä, jotka asettavat prosessille rajoituksia. Tässä väitöskirjassa tutkitiin näitä masuunille rajoituksia asettavia ilmiöitä ja pyrittiin lisäämään tietämystä niistä.

Tulokset osoittavat, että vety nopeuttaa rautaoksidien pelkistymistä alle 850 °C lämpötilassa. Suuri vesihöyrymäärä johtaa nopeaan konversioon masuunin yläkuilun aluetta vastaavassa kaasuseoksessa yli 300 °C lämpötilassa katalysoidun vesikaasun siirtoreaktion kautta. Kylmäsidottu briketti pelkistyy pellettiä nopeammin itsepelkistymisen vaikutuksesta. Briketin pelkistyesään läpikäymät faasitransformaatiot seuraavat faasien tasapainotiloja. Pelletin pehmenemisen aiheuttaa sulan muodostuminen, joka laukaisee västiin liukenemisen sitä ympäröivään sulaan kuonafaasiin.

*Asiasanat:* injektoitava pelkistysaine, korkealämpötilaominaisuudet, kosteus, kylmäsidottu briketti, masuuni, pehmeneminen, pelkistyminen, rautamalmipelletti



## Acknowledgements

The research work of this thesis was carried out in the Process Metallurgy Group of the Centre of Advanced Steel Research (CASR) at the University Oulu during 2010–2015. The research work of the thesis was made as a part of the Energy Efficiency & Lifecycle Efficient Metal Processes (ELEMET) and System Integrated Metals Processing (SIMP) research programmes coordinated by the Finnish Metals and Engineering Competence Cluster (FIMECC). The thesis has been funded by SSAB Europe Oy and the Finnish Funding Agency for Technology and Innovation (TEKES). This thesis has also been supported by scholarships awarded by Jenny ja Antti Wihurin rahasto, Tauno Tönningin Säätiö, Tekniikan Edistämissäätiö (TES) and Walter Ahlströmin Säätiö.

I would like to express my gratitude to Professor Timo Fabritius, who supervised the thesis, for giving me the opportunity to pursue a doctoral degree. Co-operation with industry had an important role in this thesis and I would like to thank Doctor Timo Paananen and Mr. Olli Mattila from SSAB Europe for their collaboration, advice and sharing of ideas during the thesis. My thanks go to Doctor Timo Paananen also for supervising the thesis. Official thesis pre-examiners Associate Professor Alexander Babich from RWTH Aachen University and Docent Lena Sundqvist-Öqvist from Luleå University of Technology are appreciated for their valuable comments and suggestions to improve the presentation of scientific work in the thesis.

I would like thank my colleagues and research group personnel for many fruitful discussions about the topics of the thesis. I thank Mr. Mikko Iljana, who worked in the same research field, for his co-operation and sharing of ideas during the thesis. Doctor Eetu-Pekka Heikkinen is appreciated for giving advice in thermodynamics. My thanks go to Mr. Tommi Kokkonen for technical support in laboratory work. Doctor Hannu Suopajarvi and Mr. Petri Sulasalmi are appreciated for some great discussions over lunch moments.

Finally, I would like to thank Sanna, my parents and friends for their encouragement and support.

Oulu, September 2015

Antti Kemppainen



## Symbols and abbreviations

$e$	Napier's constant (2.718)
$E_A$	Activation energy (kJ/mol)
$k$	Apparent rate constant
$k_0$	Frequency factor
$K_p$	Equilibrium constant
$p_i$	Partial pressure of gas $i$ (atm)
$R$	Universal gas constant (8.314 kJ/mol)
$T$	Temperature (K)
$\Delta G$	Gibbs free energy (kJ/mol)
$\Delta H$	Reaction enthalpy (kJ/mol)
$\Delta H^\circ$	Standard enthalpy of the reaction at 298 K (kJ/mol)

ARUL	Advanced reduction under load
BF	Blast furnace
BFS	Blast furnace simulator
CZS	Cohesive zone simulator
EDS	Energy dispersive spectrometer
FESEM	Field emission scanning electron microscope
GGBFS	Ground granulated blast furnace slag
GSP	Gas sampling point
HPL	Hematite pellet layer
LF	Layer furnace
LOM	Light optical microscope
MPL	Magnetite pellet layer
PC	Portland cement
RD	Reduction degree (%)
RUL	Reduction under load
TGA	Thermogravimetric analysis
WGSR	Water-gas shift reaction
XRD	X-ray diffraction
XRF	X-ray fluorescence



## List of original publications

This thesis is based on the following publications, which are referred throughout the text by their Roman numerals:

- I Kemppainen A, Mattila O, Heikkinen E-P, Paananen T & Fabritius T (2012) Effect of H<sub>2</sub>-H<sub>2</sub>O on the reduction of olivine pellets in CO-CO<sub>2</sub> gas. *ISIJ Int* 52(11): 1973–1978.
- II Kemppainen A, Alatarvas T, Iljana M, Haapakangas J, Mattila O, Paananen T & Fabritius T (2014) Water-gas shift reaction in an olivine pellet layer in the upper part of blast furnace shaft. *ISIJ Int* 54(4): 801–809.
- III Kemppainen A, Iljana M, Heikkinen E-P, Paananen T, Mattila O & Fabritius T (2014) Reduction behavior of cold-bonded briquettes under simulated blast furnace conditions. *ISIJ Int* 54(7): 1539–1545.
- IV Kemppainen A, Ohno K-I, Iljana M, Mattila O, Paananen T, Heikkinen E-P, Maeda T, Kunitomo K & Fabritius T (2015) Softening behaviors of acid and olivine fluxed iron ore pellets in the cohesive zone of a blast furnace. *ISIJ Int*. DOI: 10.2355/isijinternational.ISIJINT-2015-023.

All the publications were written by the author of this thesis. The author's main responsibilities were research design, experimental work, analytical work and reporting the results.



# Contents

<b>Abstract</b>	
<b>Tiivistelmä</b>	
<b>Acknowledgements</b>	<b>7</b>
<b>Symbols and abbreviations</b>	<b>9</b>
<b>List of original publications</b>	<b>11</b>
<b>Contents</b>	<b>13</b>
<b>1 Introduction</b>	<b>15</b>
<b>2 Background</b>	<b>17</b>
2.1 Blast furnace process .....	17
2.1.1 Iron oxide reduction .....	18
2.1.2 High H <sub>2</sub> O concentration in the upper part of the shaft .....	20
2.2 Requirements for ferrous burden in the BF process.....	21
2.2.1 Furnace shaft .....	21
2.2.2 Cohesive zone.....	23
2.3 Thesis objectives .....	24
<b>3 Experimental research</b>	<b>27</b>
3.1 Materials .....	27
3.1.1 Iron ore pellets.....	27
3.1.2 Cold-bonded briquettes .....	27
3.2 Reduction experiments.....	28
3.2.1 Sample preparation.....	28
3.2.2 Thermogravimetric analysis .....	29
3.2.3 Blast furnace simulator.....	31
3.3 Gas conversion experiments .....	33
3.4 Softening experiments.....	34
3.5 Analytical methods .....	35
3.5.1 Field emission scanning electron microscope with energy- dispersive X-ray spectroscopy.....	36
3.5.2 Gas analyser .....	36
3.5.3 Light optical microscope .....	36
3.5.4 Stereo microscope .....	37
3.5.5 X-ray diffractometer .....	37
3.5.6 X-ray fluorescence with iron content and valence analysis.....	37
<b>4 Results</b>	<b>39</b>
4.1 The effect of H <sub>2</sub> on the iron oxide reduction reactions .....	39

4.1.1	Reduction rate.....	39
4.1.2	Activation energy .....	42
4.1.3	Sample microstructure.....	44
4.2	The effect of high H <sub>2</sub> O concentration in the BF shaft.....	45
4.2.1	The WGSR in a hematite pellet layer .....	45
4.2.2	The WGSR in a magnetite pellet layer .....	50
4.2.3	Reaction rate of the WGSR .....	52
4.3	Reduction behaviour of cold-bonded briquette .....	53
4.3.1	Phase transformations.....	53
4.3.2	Reduction and swelling .....	56
4.4	Softening behaviour of iron ore pellet.....	59
4.4.1	Contraction .....	59
4.4.2	Phase evolution.....	60
<b>5</b>	<b>Discussion</b>	<b>69</b>
5.1	Iron oxide reduction in H <sub>2</sub> -H <sub>2</sub> O-CO-CO <sub>2</sub> gas .....	69
5.2	The WGSR and BF shaft conditions .....	70
5.3	High temperature properties of cold-bonded briquette .....	73
5.4	Softening mechanism of the iron ore pellet.....	75
5.5	Industrial relevance of the thesis .....	77
<b>6</b>	<b>Conclusions</b>	<b>81</b>
<b>7</b>	<b>Recommendations for future work</b>	<b>83</b>
	<b>References</b>	<b>85</b>
	<b>Original publications</b>	<b>91</b>

# 1 Introduction

The Blast Furnace (BF) process remains the most common process in the world for making iron. Iron ore (iron oxides) and coke are the main raw materials of the BF process which are charged on top of the shaft furnace. Hot metal is produced in the BF process from iron oxides through reduction reactions achieved with coke, injected reductants and hot air blast. Coke is the primary reductant of the BF and it provides the heat to the process via the combustion reaction with oxygen ( $O_2$ ) of the blast air. Reactions between  $O_2$  and coke form carbon monoxide (CO) which is the primary reducing agent for iron oxides in the BF process.

Carbon dioxide ( $CO_2$ ) emission limits bring new challenges to steel companies demanding more and more efficient process optimisation and utilisation of by-products. Coke is the primary source for  $CO_2$  emissions in steel plants and coke consumption is commonly reduced by replacing part of it with injected reductants such as oil, plastic and pulverised coal. The combustion of injected reductants releases hydrogen ( $H_2$ ) which acts as a reducing agent replacing part of CO in the reducing gas. A high rate of injected reductants alters the concentrations of  $H_2$  and  $H_2O$  gases in the BF shaft and therefore changes the composition of the reducing gas. Iron oxide reduction by CO differs from reduction by  $H_2$  which has an effect on the iron oxide reduction reactions.  $H_2$  forms water vapour ( $H_2O$ ) as a result of iron oxide reduction increasing the concentration of  $H_2O$  in the upper part of the BF shaft.

In an effort to reach  $CO_2$  emission limits, the sintering plant at SSAB Europe Raahе steelworks in Finland was shut down. Due to this change, the charging procedure of iron oxides has been changed from mixed sinter and pellet to mixed pellet and cold-bonded briquette. The change of the BF charging procedure has various effects on the process since the amount of the pellets is considerably increased and a cold-bonded briquette is introduced as a new burden material. The change requires extensive laboratory and pilot-scale testing.

The transition to the use of pellets and cold-bonded briquettes in the BF increases the moisture content of the burden since the burden materials are stored partly outdoors. This chemically unbound  $H_2O$  of the burden is volatilised by the heat of the top gas in the upper part of the shaft. In addition, the briquettes contain hydrated, chemically bound water which vaporises in the shaft in the hydrate decomposition reactions. These both increase the content of  $H_2O$  in the upper part of BF shaft. The high  $H_2O$  concentration in the upper part of the shaft affects the

gas phase reactions and makes reactions such as the Water-Gas Shift Reaction (WGSR) more intensive.

The ferrous BF burden material has to fulfil the requirements needed for smooth BF operation. Formation of fines disturbs the flow of the reducing gases and decreases furnace efficiency. The location, shape and thickness of the cohesive zone all have a significant effect on BF efficiency and it is affected by the softening and melting properties of the ferrous burden. In the BF with mixed pellet and briquette charging, furnace efficiency is dependent on the high temperature properties of the pellet and the cold-bonded briquette.

The high rate of injected reductants, burden water content and high temperature properties of the burden materials cause various phenomena in the BF process which set limitations to the process. These limiting phenomena are studied in this doctoral thesis. The research work of the thesis is carried out through laboratory experiments which simulate the conditions of the actual BF. Novel experimental methods are used to study the phenomena related to iron production in the BF process with pellet charging. New knowledge is obtained about the fundamentals of the limiting phenomena related to the use of pellets in the BF process.

## 2 Background

### 2.1 Blast furnace process

The BF is the most common process for making iron in the world. Metallic iron is produced in the BF from iron ore which consists of iron oxides and gangue minerals. The BF process is based on a removal of oxygen from the iron oxides which leads to production of hot metallic iron as the main product of the process. The BF is a counter current shaft furnace where iron oxides and coke are charged in alternate layers from the top of the furnace. Iron oxides are commonly charged in the form of sinter, pellet or lump ore. Hot air with oxygen enrichment is blown in the BF through the tuyeres located in the lower part of the furnace. The BF process is illustrated in Fig. 1. Reaction between coke and oxygen of the hot air in the “raceway” region heats the gas up to 2200 °C providing the required energy for the process. Alternative reductants, such as pulverised coal, oil or plastic are commonly injected through the tuyeres to replace part of the expensive metallurgical coke.

The BF is an efficient heat and mass transfer reactor where the solid burden descends in the shaft and the ascending hot gas heats up and reacts with the charged burden. Metallic iron is produced from the iron oxides through reduction reactions with reducing gas which is formed from coke, injected reductants and hot air blast. Coke and injected reductants act as a fuel and reducing agent in the BF releasing carbon monoxide and hydrogen in the ascending gas after reaction with oxygen. CO and H<sub>2</sub> components of the ascending gas decrease the amount of oxygen in iron oxides and finally reduce them to metallic iron at high temperature. Reduction of iron oxides occurs partly via indirect reactions with gas and partly via direct reduction with coke. The indirect reduction is more energy efficient and therefore preferred. A high amount of indirect reduction indicates high utilisation of reducing gas. Thus, the permeability of the BF burden should be as high as possible to enable intimate contact between burden and gas to increase furnace efficiency. (Geerdes *et al.* 2009).

The iron ore burden starts to soften and melt in the cohesive zone of the BF at 1100 °C as shown in Fig. 1. A BF slag is formed from the gangue of the burden and added fluxes. Molten iron and slag drip in the BF heart where molten slag floats on the molten iron. The molten iron and the slag are tapped out via separate tap holes located at the bottom of the furnace.

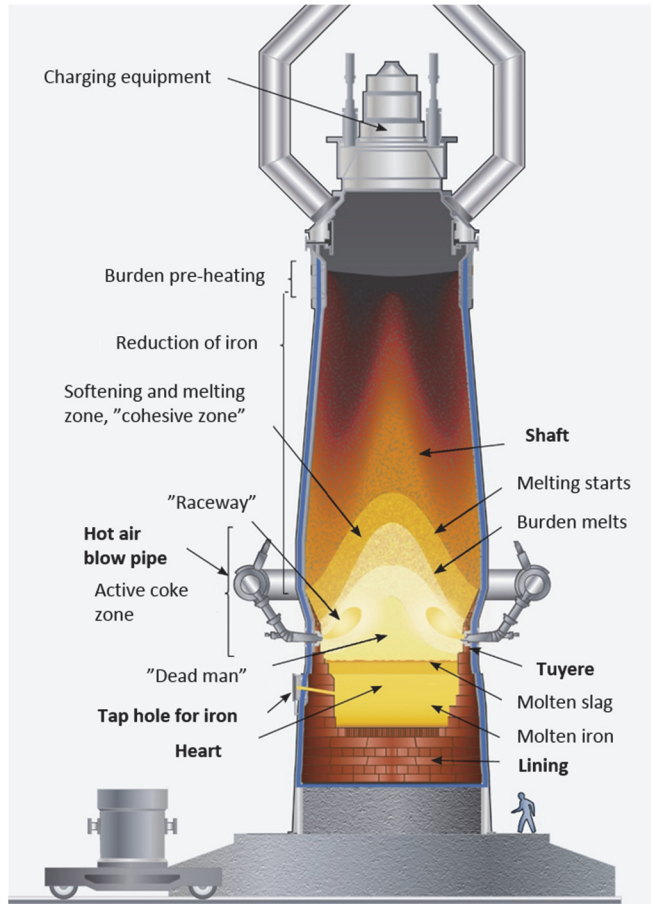


**Fig. 1. The blast furnace process (Teräskirja 2014, reprinted by permission of Metallinjalostajat ry).**

### **2.1.1 Iron oxide reduction**

In a BF where pellet is used, the ferrous burden consists mainly of iron ore pellets. The pellets are produced in a pelletising process which is presented in the literature (Babich *et al.* 2008). The iron oxide which is charged in the form of pellets consists typically of hematite ( $\text{Fe}_2\text{O}_3$ ) with a small percentage of magnetite ( $\text{Fe}_3\text{O}_4$ ). The reduction reactions of iron oxides start in the BF at around 500 °C with hematite to magnetite reduction. At 600–800 °C, the magnetite to wüstite ( $\text{FeO}$ ) reduction step takes place. At 800–1150 °C the wüstite is reduced to partly metallic iron (Fe). The

region at between 500 and 1150 °C in the BF shaft is called the indirect reduction zone where the burden is reduced via gas-solid reactions by the reducing gas generated at the “raceway”. The remaining iron oxides are reduced to metallic iron in a direct reduction with coke mainly above 1150 °C. According to Geerdes *et al.* (2009), the iron oxides are reduced at the following temperatures in the BF shaft:

- Fe<sub>2</sub>O<sub>3</sub> to Fe<sub>3</sub>O<sub>4</sub> at 500–600 °C
- Fe<sub>3</sub>O<sub>4</sub> to FeO at 600–800 °C
- FeO to FeO<sub>½</sub> at 800–1150 °C
- FeO to Fe at above 1150 °C

The iron oxides are reduced either by CO, H<sub>2</sub> or coke (C) producing CO<sub>2</sub> and H<sub>2</sub>O. Iron oxide reduction reactions are shown in Eqs. 1–7:



Large amounts of injected reductants are commonly used in the BF process to reduce coke consumption. This procedure alters the gas composition in the BF shaft, where the reduction of iron oxides takes place. At high injection levels the concentrations of H<sub>2</sub> and H<sub>2</sub>O gases change in the reducing gas atmosphere, which makes it important to investigate the effects of these gases on the reduction of iron oxides in a CO-CO<sub>2</sub> atmosphere. Several studies have been conducted on reduction of iron oxides in CO (El-Geassy *et al.* 1977, El-Geassy 1986, Mondal *et al.* 2004), H<sub>2</sub> (Sastri *et al.* 1982, Turkdogan & Vinters 1972) or CO-H<sub>2</sub> mixtures (El-Geassy *et al.* 1977, Towhidi & Szekely 1981). It has been shown that the addition of H<sub>2</sub> to CO atmosphere speeds up the reduction of iron oxides when pure reductive gases are used (El-Geassy 1986, Moon *et al.* 1998, Towhidi & Szekely 1981). Various activation energies have been reported in the literature for iron oxide reduction with CO, H<sub>2</sub> and CO-H<sub>2</sub> gases, mainly on account of the different conditions under which the reduction experiments have taken place.

The atmosphere in the actual BF consist of N<sub>2</sub>, CO, CO<sub>2</sub>, H<sub>2</sub> and H<sub>2</sub>O gases where CO and H<sub>2</sub> act as reducing agents. Therefore, it is necessary to study the

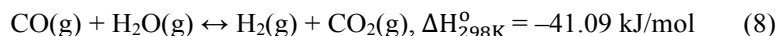
reduction of iron oxides in a gas including all gas components. In this thesis, the reduction of iron oxides was conducted under equilibrated CO-CO<sub>2</sub> and H<sub>2</sub>-H<sub>2</sub>O-CO-CO<sub>2</sub> gases in conditions which have not been investigated in the literature earlier. The effect of H<sub>2</sub> on the iron oxide reduction is shown. Reduction experiments were conducted under isothermal conditions in the range of 700–1150 °C with H<sub>2</sub>/H<sub>2</sub>O and CO/CO<sub>2</sub> ratios which simulate three different regions of the indirect reduction zone in the BF shaft. The activation energies were determined for hematite to magnetite reductions. (Paper I).

### **2.1.2 High H<sub>2</sub>O concentration in the upper part of the shaft**

Due to partial replacement of carbonaceous reductants by hydrogen bearing injected reductants, H<sub>2</sub> and H<sub>2</sub>O concentrations are increased in the BF shaft. The H<sub>2</sub>O concentration is increased in the upper part of the shaft due to iron oxide reduction by H<sub>2</sub> which is shown in Eqs. 2, 4 and 6. In the BF with pellet charging, the burden typically contains moisture due to the outdoor storage of pellets and briquettes. This chemically unbound water is evaporated in a pre-heating stage on top of the shaft as shown in Fig. 1. However, it has been shown that a high moisture content in the burden may have an effect on the temperature profile of the BF shaft (Ritz *et al.* 2004). If all the moisture is not evaporated in the pre-heating stage, it will increase the H<sub>2</sub>O content in the upper part of the shaft.

Studies have been made on the effects of H<sub>2</sub> or H<sub>2</sub>O additions on the reducing gas (El-Geassy 1986, Kemppainen *et al.* 2012, Murakami *et al.* 2012). However, authors have noticed that a remarkable increase of H<sub>2</sub>O concentration in the BF shaft has other effects in the BF shaft. One is the Water-Gas Shift Reaction (WGSR), which becomes more significant with an increasing H<sub>2</sub>O concentration in the reducing gas (Murakami *et al.* 2012, Nogami *et al.* 2012, Usui *et al.* 2002).

The WGSR, presented in Eq. 8, is a reversible, equilibrium controlled exothermic chemical reaction, usually assisted by a catalyst, and is the reaction of water vapour with carbon monoxide to produce carbon dioxide and hydrogen gas. The reaction is not affected by pressure (Martos *et al.* 2009, Newsome 1980, Rhodes *et al.* 1995, Satterfield 1991, Smith *et al.* 2010). Calculated  $\Delta G = 0$  for the WGSR via HSC Chemistry software is approximately at 810 °C and at higher temperatures the reaction towards the reactants is favourable (Roine 2009).



The WGSR is normally utilised in hydrogen production processes in a so-called high temperature shift which is conducted at a temperature range from 350 °C to 600 °C. The catalyst is typically magnetite ( $\text{Fe}_3\text{O}_4$ ), the stable iron oxide phase which under reaction conditions and combined with chromium oxide, minimizes catalyst sintering. The magnetite used as the catalyst is produced by reducing hematite. (Martos *et al.* 2009, Newsome 1980, Rhodes *et al.* 1995, Satterfield 1991, Smith *et al.* 2010). The hematite-magnetite reduction step is a sub-process in the conversion of hematite to metallic iron ( $\text{Fe}_2\text{O}_3$ - $\text{Fe}_3\text{O}_4$ - $\text{FeO}$ - $\text{Fe}$ ) in the BF process as shown in Eqs. 1 and 2. According to the general understanding of the temperature and CO-CO<sub>2</sub> gas composition profile in the BF shaft, the conditions lead to hematite to magnetite reduction reactions in the upper BF shaft area (Beppler *et al.* 1998, Kasai & Matsui 2004, Peters *et al.* 1994).

In the SSAB steel plant, a change has been detected in the measured utilisation efficiency of H<sub>2</sub> in the BF after transition to pellet charging. Gas conversion is suspected for this phenomenon. The gas conversion caused by the WGSR may have an effect on the composition of the reducing gas and therefore affect the reduction reactions and the utilisation of the BF top gas. In this thesis, the effect of the WGSR on the gas conversion at high H<sub>2</sub>O concentration is investigated by experimental methods. Experiments are conducted in a hematite pellet layer and in a magnetite pellet layer under conditions which simulate the upper part of the BF shaft. (Paper II).

## **2.2 Requirements for ferrous burden in the BF process**

### **2.2.1 Furnace shaft**

Ferrous BF burden material has to fulfil the mechanical, chemical and thermal requirements needed for smooth BF operation. The charged material has to form a strong and permeable structure to carry the burden and allow the passage of the reducing gas in the BF shaft, respectively. The early disintegration of burden has to be avoided because the formation of fines disturb the reducing gas flow in the shaft thereby decrease the process efficiency. Therefore the fine iron ore is agglomerated to a larger size before charging it to the BF. This thesis focuses on the BF process where iron ore pellets and cold-bonded briquettes are used as iron bearing materials.

Iron ore pellet is pelletised and sintered from iron ore concentrate in a pelletising process. Agglomeration of dusts and other materials into briquettes,

where cement is used as a binding material, is a commonly used method to enable by-product charging to the BF (Nakano *et al.* 2004, Singh & Björkman 2004, Singh & Björkman 2006, Singh & Björkman 2007a, Singh & Björkman 2007b). These by-products are formed in different stages of the steel production chain. The briquettes contain embedded carbon (Gudenau *et al.* 2000). A feasible option to reduce cement consumption is to replace it partly by Ground Granulated Blast Furnace Slag (GGBFS) (Chidiac & Panesar 2008, Escalante *et al.* 2001, Mäkelä *et al.* 2012, Osborne 1999). Required mechanical properties of the briquette are achieved by sufficiently long curing time periods (Mäkelä *et al.* 2012). Mechanical strength is also dependent on the source of embedded carbonaceous material (Kowitwarangkul *et al.* 2014).

A couple of standardised industrial tests have been developed to evaluate the burden reduction properties in isothermal reduction conditions. ISO 7215:2007 is a test for pellet reducibility properties. ISO 13930:2007 is a standard test to measure the degree of the size degradation of iron ore agglomerates in the low temperature reduction zone of a blast furnace. ISO 4698:2007 provides a standard for measuring the free-swelling index when pellets are reduced in an unconstrained bed under conditions resembling those in the reduction zone of a blast furnace. Because the conditions in the actual BF are not isothermal, dynamic reduction tests have been introduced recently which simulate the iron oxide reduction in the increasing temperature and changing gas atmosphere of the BF shaft (Iljana *et al.* 2012). There is no standardised reduction test available for the briquettes.

The iron ore pellets swell while being reduced in the BF process as a result of reduction reactions. The increased porosity of pellets as a normal swelling can be considered advantageous for the reduction process, but abnormal swelling of the pellets is unfavourable, thus increasing the generation of dust and fines (Iljana *et al.* 2012). Abnormal swelling has been detected also with cold-bonded briquettes, but not with lump ore or sinter (Singh & Björkman 2007b). This thesis focuses on the reduction behaviour of the cold-bonded briquette.

The chemical composition of the cold-bonded by-product briquette differs considerably from iron ore pellet or sinter. The briquette is usually rich with carbon, iron oxides and calcium oxides. Various reactions such as decomposition of the cement phases, the gasification of carbon and the reduction of iron oxides take place in the BF. This leads to various phase transformations and metamorphosis in the briquette. (Robinson 2005, Robinson *et al.* 2011). The durability of the briquette in the BF conditions is dependent on these phase transformations. Tendency for catastrophic reduction swelling has been detected in some occasions (Singh &

Björkman 2007b). These issues make the reduction behaviour experiments necessary.

In this thesis, the cold-bonded briquettes were reduced under a dynamic reduction programme which simulates the indirect reduction zone up to 1100 °C in the BF shaft. The reduction behaviour of a cold-bonded briquette is studied and compared to an iron ore pellet which is used as a reference sample. In addition, the effect of GGBFS as a cement replacement is investigated. (Paper III).

### **2.2.2 Cohesive zone**

The softening and melting of the burden occur in the cohesive zone of the BF at above 1100 °C. The softening and melting makes the burden impermeable which directs the gas to flow through coke layers. The loss of permeability is caused by melt onset and deformation of the solid phases due to the pressure of the burden. Molten iron drips in the heart of the BF from the cohesive zone. The loss of permeability causes significant pressure drop in the BF process which has an effect on BF efficiency. The gaseous reduction of iron oxides by CO is more energy efficient than direct reduction by coke due to exothermic nature of gaseous reduction reactions and the endothermic nature of the direct reduction reaction (Walker 1986). Therefore, the region of the exothermic indirect reduction zone should be large compared to the endothermic direct reduction zone to reach low coke consumption (Babich *et al.* 2008). Thus, it is favourable for the blast furnace process that the gas-impermeable layer is formed at a high temperature, since it provides more space for gaseous reduction (Sterneland *et al.* 2003).

Typically the burden cohesive zone behaviour is tested by softening and melting experiments. Reduction under Load (RUL) is a standardised industrial test (ISO 7992:2007) which provides a relative measure for evaluating the structural stability of iron ores, when reduced under conditions prevailing in the reduction zone of a blast furnace. RUL is an isothermal test. The recently introduced Advanced Reduction Under Load (ARUL) industrial test simulates the BF conditions step wisely simulating the conditions more accurately (Iljana *et al.* 2015a).

A Reduction Degree (RD) of a ferrous burden is typically above 50% in the cohesive zone area of a BF (Bakker 1999). At this point the iron bearing burden consists of metallic iron, wüstite and other oxides which form a slag phase. The phase compositions are dependent on the chemistry of the iron bearing burden. Thus, the softening properties of various iron ore burden materials (sinter, pellet,

lump) differ from each other markedly. (Barnaba 1985, Borinder & Bi 1989, Kaushik & Fruehan 2006a). Variables such as the RD, basicity, gangue content, slag viscosity etc. have an effect on the softening and melting properties. The occurrence of many simultaneous phenomena during the softening and melting makes the clarification of these effects difficult. (Bakker 1999, Borinder & Yang 1987, Kaushik & Fruehan 2006b, Nogueira & Fruehan 2004, Nogueira & Fruehan 2005, Nogueira & Fruehan 2006).

In this thesis, the softening behaviour of iron ore pellets was studied using a laboratory scale Cohesive Zone Simulator (CZS) in an inert atmosphere. The effect of pre-reduction on the softening behaviour is investigated with commercial grade acid and olivine fluxed pellets. The phenomena causing the deformation of the pellet are sought from its microstructure. The results were analysed with the assistance of computed thermodynamic calculations. (Paper IV).

### **2.3 Thesis objectives**

The high  $H_2$  and  $H_2O$  concentrations affect the iron oxide reduction reactions and gas phase reactions in the BF. There have been indications that they may have an effect on process variables such as the measured utilisation efficiency of  $H_2$  in the actual BF process causing error. All the effects of high  $H_2$  and  $H_2O$  concentrations in the BF are not known.

The high temperature properties (reducibility, swelling, softening etc.) of the burden has an effect on the flow of the reducing gas and the formation of cohesive zone. They affect significantly the efficiency of the indirect reduction zone which determines the share of unreduced material which descends lower in the BF. Direct reduction by coke consumes more energy than indirect reduction by gas and has an effect on the efficiency of the BF process.

The phenomena which were studied in this thesis have significant effects on the actual BF process with pellet charging. These phenomena affect BF operation practices and cause limitations to the process. The aim of this thesis was to clarify these phenomena and to obtain new knowledge about the mechanisms behind them. The thesis objectives are illustrated in Fig. 2. The following Research Questions (RQ) set the objectives of this thesis:

RQ 1: The effect of  $H_2$  on the iron oxide reduction reactions in the indirect reduction zone of the BF.

RQ 2: The effect of high  $H_2O$  concentration in the upper part of the BF shaft.

RQ 3: The reduction behaviour of a cold-bonded briquette in the indirect reduction zone of the BF.

RQ 4: The softening behaviour of acid and olivine fluxed iron ore pellets in the cohesive zone of the BF.

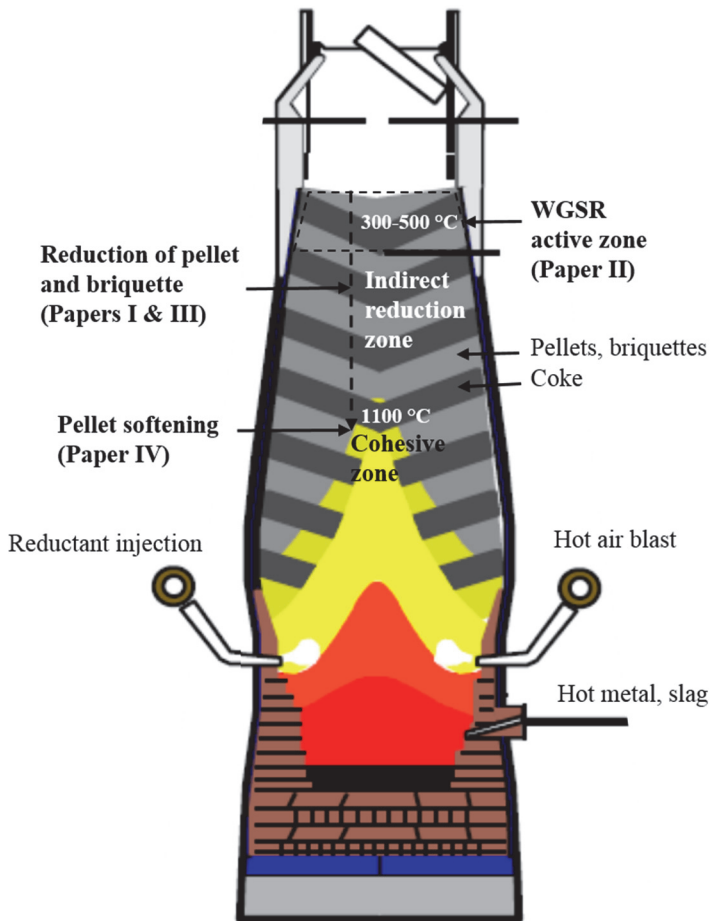


Fig. 2. Illustration of the thesis objectives.



## 3 Experimental research

### 3.1 Materials

#### 3.1.1 Iron ore pellets

Commercial grade acid and olivine fluxed iron ore pellets for blast furnaces were used as samples in the laboratory experiments of the thesis. The pellets were in the size range of 10–15mm in diameter. Chemical composition, basicity and amount of slag formers of the pellets are shown in Table 1. It was required to decrease the divalent iron ( $\text{Fe}^{2+}$ ) content of the samples for some of the experiments and therefore a fraction of the olivine fluxed pellets was magnetically separated. These olivine fluxed pellets containing low amounts of magnetite are named as “Low mag. olivine” in Table 1.

**Table 1. Chemical composition, basicity and amount of slag formers of the iron ore pellets.**

Component (wt-%)	Acid	Low mag. olivine	Olivine
$\text{Fe}_{\text{tot}}$	65.4	67.1	66.8
FeO	1.4	0.1	0.4
MgO	0.16	1.25	1.3
$\text{Al}_2\text{O}_3$	0.29	0.3	0.36
$\text{SiO}_2$	5.27	1.69	1.84
CaO	0.49	0.38	0.41
$\text{K}_2\text{O}$	0.111	n.a.	0.019
$\text{Na}_2\text{O}$	0.052	n.a.	0.039
S	0.01	0	0.001
Slag formers (wt-%)	6.37	3.62	3.97
CaO/ $\text{SiO}_2$	0.09	0.22	0.22

#### 3.1.2 Cold-bonded briquettes

The cold-bonded briquettes which were investigated in this work were produced in SSAB Europe Raahe steelworks in Finland. The chemical composition of the cold-bonded briquette is shown in Table 2.

**Table 2. Chemical composition of the cold-bonded briquette (wt-%) (Paper III, reprinted by permission of ISIJ International).**

H <sub>2</sub> O	S	MgO	Al <sub>2</sub> O <sub>3</sub>	SiO <sub>2</sub>	CaO	Ti	V	Mn	Fe	C
5.68	0.3	1.12	1.44	7.13	13.86	0.21	0.16	0.57	49.25	10.75

Table 3 shows all the sample materials which were used in the laboratory experiments of the thesis and the papers (I–IV) where the original work is presented.

**Table 3. Materials used in the laboratory experiments of the thesis and the papers (I–IV) where the original work is presented.**

	Low mag. olivine pellet	Olivine pellet	Acid pellet	Cold-bonded briquette
The effect of H <sub>2</sub> on the iron oxide reduction	I			
The effect of high H <sub>2</sub> O concentration	II			
Reduction behaviour of cold-bonded briquette		III		III
Softening behaviour of iron ore pellet		IV	IV	

## 3.2 Reduction experiments

### 3.2.1 Sample preparation

Individual iron ore pellets shown in Table 1 were used as test samples. The briquette samples were prepared for the experiments by cutting an industrial scale cold-bonded briquette in 12 triangle shaped pieces as illustrated in Fig. 3. The weight of each briquette sample was between 36 and 41 grams. The cold-bonded briquette samples contained Portland Cement (PC) and Ground Granulated Blast Furnace Slag (GGBFS) as binders as shown in Table 4.

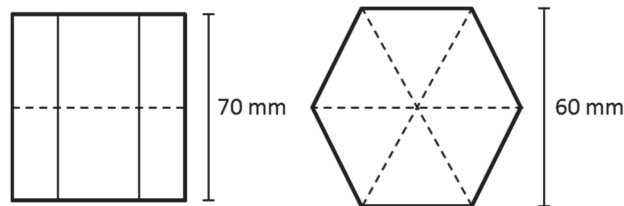


**Fig. 3. Illustration of the briquette sample preparation (Paper III, reprinted by permission of ISIJ International).**

**Table 4. Binders of the briquette samples (Paper III, reprinted by permission of ISIJ International).**

Sample	Binder material (wt-%)
0, 00	10% PC
3	8% PC + 3% GGBFS
6	8% PC + 6% GGBFS

### **3.2.2 Thermogravimetric analysis**

Thermogravimetric analysis (TGA) furnace was used to study the effect of H<sub>2</sub> on the reduction of iron oxides. The TGA furnace is illustrated in Fig. 4. A low magnetite containing olivine pellet (Table 1) was used as a sample in each experiment. Pellets weighing 4.0–4.3 grams were used in the experiments in order to enhance comparison. A couple of preliminary repetition tests showed no significant differences in the reduction behaviour of pellets weighing 4.0–4.3 grams. The experiments were performed in equilibrated CO-CO<sub>2</sub> and H<sub>2</sub>-H<sub>2</sub>O-CO-CO<sub>2</sub> gases where the reduction potentials of CO and H<sub>2</sub> were set to equal. The conditions of the performed reduction experiments are shown in Table 5. More details about the conditions of the thermogravimetric reduction experiments are presented in Paper I.

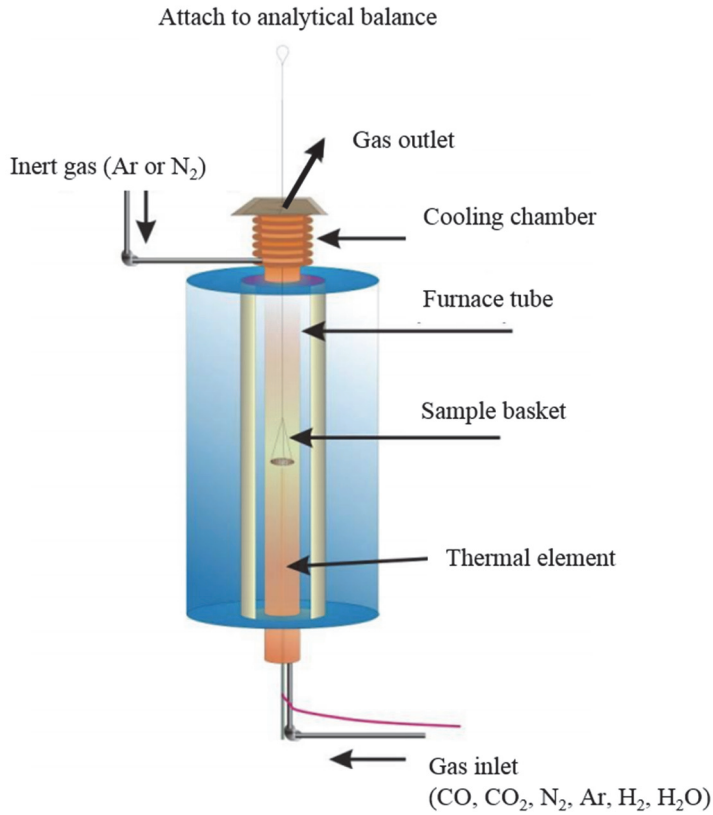


**Fig. 4. Illustration of the TGA furnace.**

**Table 5. Compositions of the gas mixtures, gas flow rates and temperatures used in the reduction experiments (Paper I, reprinted by permission of ISIJ International).**

Experiment	1	2	3	4	5	6	7	8	9	10	11	12
H <sub>2</sub> (%)							1.1	1.1	1.1	1.1	4.2	6.4
H <sub>2</sub> O (%)							6.9	6.9	6.9	6.9	3.8	1.6
CO (%)	15	15	15	15	65	90	13.8	13.8	13.8	13.8	59.8	82.8
CO <sub>2</sub> (%)	85	85	85	85	35	10	78.2	78.2	78.2	78.2	32.2	9.2
Time (min)	60	60	60	60	60	60	60	60	60	60	60	60
Flow (l/min)	2	2	2	2	2	2	2	2	2	2	2	2
T (°C)	750	800	850	900	1000	1150	750	800	850	900	1000	1150

### 3.2.3 Blast furnace simulator

A Blast Furnace Simulator (BFS) was used to study the reduction behaviour of the cold-bonded briquettes under dynamic reduction conditions. A schematic diagram of the BFS equipment is presented in Fig. 5. The experimental conditions in the BFS simulate the indirect reducing zone of the BF shaft. Dynamic programmes were used to study the reduction and phase transformations in the briquettes when the iron oxides were reduced to iron oxide phase stability areas of magnetite, wüstite and iron. The experiments were labelled as “Magnetite”, “Wüstite”, “Iron 1” and “Iron 2” according to these phase stability areas. The gas atmosphere and temperature profiles of the conducted experiments are shown in Fig. 6. The reducing conditions are illustrated in Fe-O-CO-CO<sub>2</sub> phase diagram in Fig. 7.

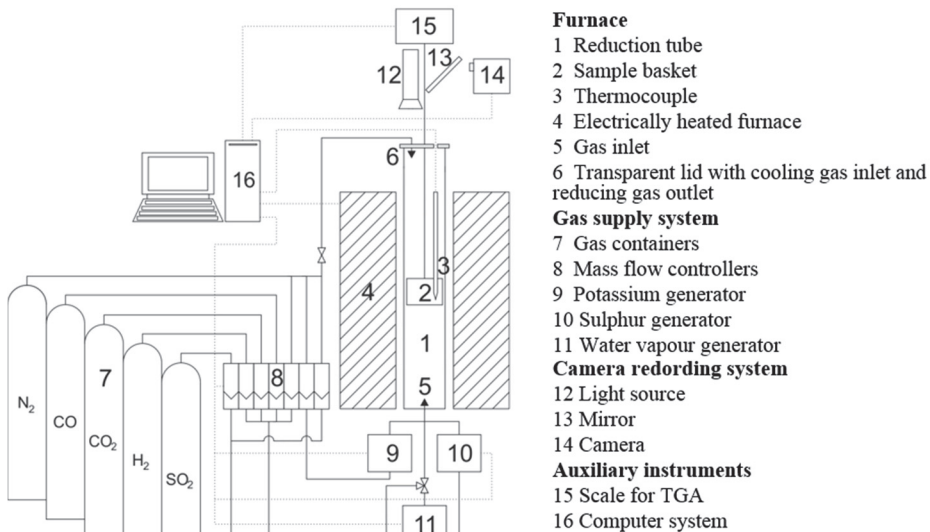


Fig. 5. Schematic diagram of the blast furnace simulator (Iljana *et al.* 2012, reprinted by permission of ISIJ International).

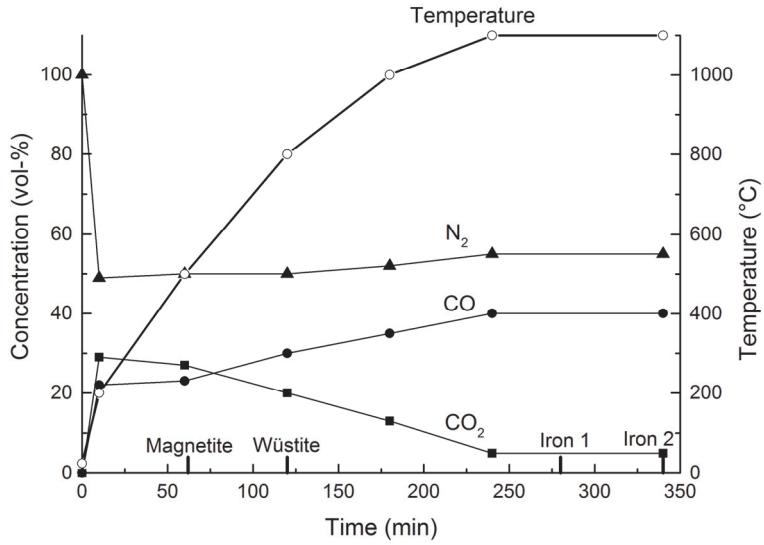


Fig. 6. Gas atmosphere and temperature profiles presented as a function of time in the experiments (Ilijana *et al.* 2012, reprinted by permission of ISIJ International).

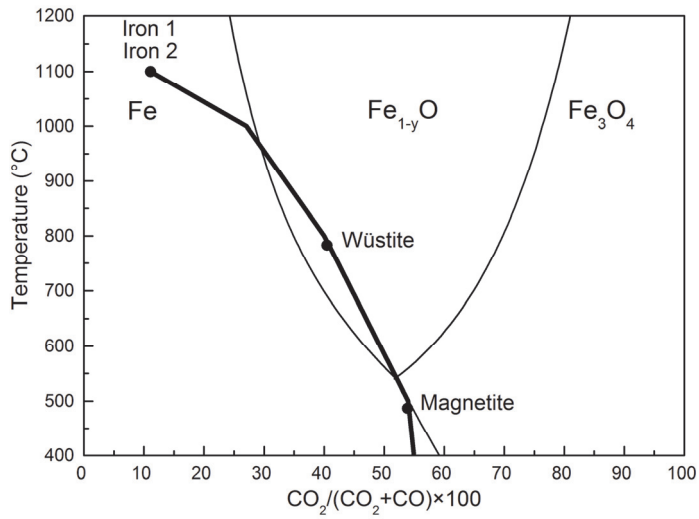
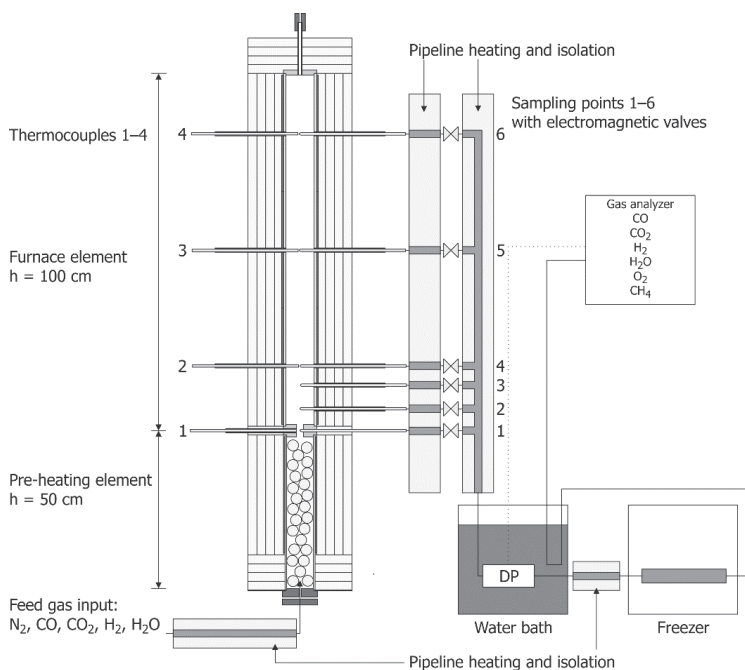


Fig. 7. Reducing conditions in the experiments shown in a Fe-O-CO-CO<sub>2</sub> phase diagram (Ilijana *et al.* 2012, reprinted by permission of ISIJ International).

### 3.3 Gas conversion experiments

The effect of high H<sub>2</sub>O concentration was investigated by Layer Furnace (LF) experiments. The LF is illustrated in Fig. 8 and was originally presented by Alatarvas *et al.* (2012). An arbitrary atmosphere profile can be set to the LF consisting of N<sub>2</sub>, CO, CO<sub>2</sub>, H<sub>2</sub> and H<sub>2</sub>O gas components. The furnace tube, having a diameter of 80 mm, can be loaded with a 1.0 m high bed of desired materials and heated up to 1200 °C. The LF is equipped with a gas analyser. A detailed description of the LF is presented in Paper II. In the present experiments, the tube was filled with hematite pellets (Table 1). Gas analyses were taken from the Gas Sampling Points (GSP). The analyses of GSPs 1–4 were used in the experiments of the thesis. Gas conversions were measured in a Hematite Pellet Layer (HPL) and in a Magnetite Pellet Layer (MPL). The conditions of the conducted experiments are shown in Table 6 and illustrated in Fe-C-H-O phase diagram in Fig. 9. The Fe-C-H-O phase diagram was drawn by the method of Oeters *et al.* (2011).



**Fig. 8. Schematic illustration of the layer furnace (Paper II, reprinted by permission of ISIJ International).**

**Table 6. Conditions in the LF experiments (Paper II, modified and reprinted by permission of ISIJ International).**

Experiment	HPL	MPL
H <sub>2</sub> (%)	0	0
H <sub>2</sub> O (%)	8	8
CO (%)	17	17
CO <sub>2</sub> (%)	25	25
N <sub>2</sub> (%)	50	50
Gas flow rate (l/min)	15	15
Heating rate (°C/min)	3	3
Max temperature (°C)	500	500
Height of the packed bed (m)	1	1
Time held at max temp. (min)	150	150

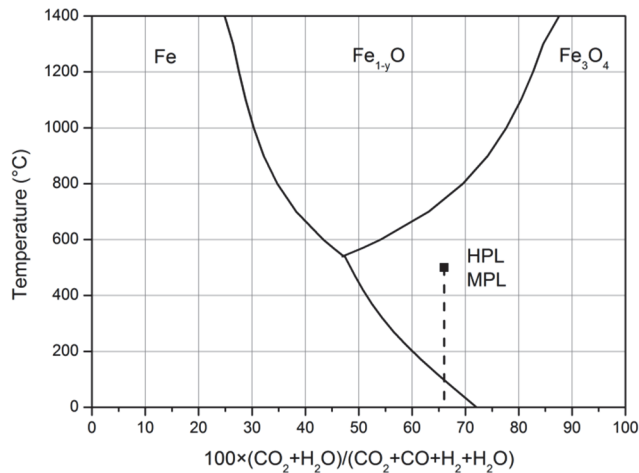


**Fig. 9. Conditions of the LF experiments shown in Fe-C-H-O phase diagram (Paper II, reprinted by permission of ISIJ International).**

### 3.4 Softening experiments

The softening behaviour of the acid and the olivine fluxed iron ore pellets were investigated using a Cohesive Zone Simulator (CZS). A schematic layout of the CZS equipment is shown in Fig. 10. The CZS experiments were conducted in an inert atmosphere (N<sub>2</sub>) at a heating rate of 10 °C/min. A single pellet was used as a sample in each experiment. The pellets were pre-reduced to RDs of 50–70% by the

BFS before the softening tests. Detailed descriptions of the pre-reduction, CZS equipment and experimental conditions are presented in Paper IV.

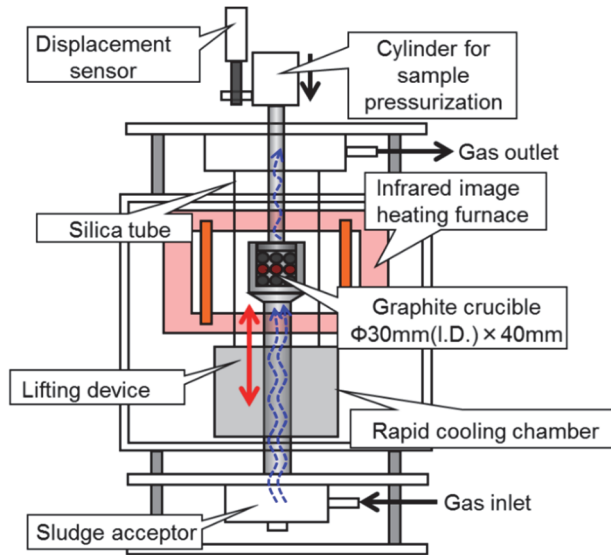


**Fig. 10. A schematic layout of the cohesive zone simulator (Paper IV, reprinted by permission of ISIJ International).**

### 3.5 Analytical methods

Chemical analysis of the untreated samples was made by X-Ray Fluorescence (XRF) techniques. After the reduction and softening experiments, the samples were sunk in epoxy, cut and polished for microstructural analysis. Polished sections of the samples were observed visually by using a Light Optical Microscope (LOM). The phase compositions of the polished samples were analysed using Field Emission Scanning Electron Microscope equipped with Energy-Dispersive X-ray Spectroscopy (FESEM-EDS). Chemical compositions of the powdered samples were analysed by X-Ray Diffraction (XRD). All the analytical methods which were used in the thesis are shown in Table 7.

**Table 7. All the analytical methods used in the thesis.**

Paper	I	II	III	IV
FESEM-EDS	x			x
Gas analyser		x		
LOM	x		x	x
Stereo microscope				x
XRD			x	
XRF	x	x	x	x

### ***3.5.1 Field emission scanning electron microscope with energy-dispersive X-ray spectroscopy***

Zeiss Ultra Plus FESEM with Oxford Inca software was used to identify the phase compositions in the samples. Polished samples were coated with thin layer (0.2 mm) of carbon to ensure the electric conductivity which is necessary for the FESEM-EDS analysis. All the analyses were taken by a point analysis method using backscatter image setting. Operating parameters of the FESEM equipment were 15kV EHT, 2.3 nA current, 60.0  $\mu\text{m}$  aperture and 8.5 mm working distance.

### ***3.5.2 Gas analyser***

A Portable Infrared Coal gas Analyser Gasboard-3100P made by Wuhan Cubic Optoelectronics Co., Ltd. was used for the gas conversion measurements in the LF experiments. A detailed description of the gas measurement procedure in the conducted experiments is found in Paper II.

### ***3.5.3 Light optical microscope***

Optical examination of the polished samples was made by using Olympus BX51 LOM equipped with camera. The optical microscope was used as a part of the microstructural analysis to visually study the structures and phases in the samples. Objectives with magnifications of 40, 100, 200 and 500X were used.

### **3.5.4 Stereo microscope**

An Olympus SZX9 zoom stereo microscope was used to capture macroscopic images of single pellets. The microscope has a zoom ratio of 1:9.05 and magnification range of 0.63–5.7X.

### **3.5.5 X-ray diffractometer**

Crystallographic analysis of the powder samples were made by using Siemens D5000 powder X-Ray diffractometer with Cu anode tube  $K_{\alpha}$  ( $\lambda = 1.542 \text{ \AA}$ ). A graphite secondary monochromator was used in the measurements. Phases were identified from the diffraction pattern with Bruker AXS Ddifrac<sup>plus</sup> Eva 12 software using ICDD PDF-2 database. The samples were ground and sieved to a particle size smaller than 500  $\mu\text{m}$  for the XRD analysis.

### **3.5.6 X-ray fluorescence with iron content and valence analysis**

The X-ray fluorescence method was used for the bulk chemical analysis. Philips PW 2404 equipment. The iron content measurement method has been presented in the thesis of Paananen (2013).



## 4 Results

### 4.1 The effect of H<sub>2</sub> on the iron oxide reduction reactions

#### 4.1.1 Reduction rate

The effect of H<sub>2</sub> on the iron oxide reduction was investigated with equilibrated H<sub>2</sub>-H<sub>2</sub>O-CO-CO<sub>2</sub> and CO-CO<sub>2</sub> gases. The effects of the H<sub>2</sub>-H<sub>2</sub>O additions on the rate of reduction of the iron ore pellets in the CO-CO<sub>2</sub> mixtures are shown in Figs. 11–13. The reduction (%) corresponding to the reduction degree (%) is calculated in Eq. 9.

$$\text{Reduction (\%)} = \frac{\text{Weight of oxygen removed from iron oxides}}{\text{Total weight of removable oxygen in iron oxides}} \quad (9)$$

An 8 vol-% H<sub>2</sub>-H<sub>2</sub>O addition to the CO-CO<sub>2</sub> mixture at a fixed ratio increases the reduction rate at temperatures of 750 and 800 °C, as shown in Fig. 11. At 850 °C, the reduction rate is increased slightly by the H<sub>2</sub>-H<sub>2</sub>O addition as shown in Fig. 12. At 900 and 1000 °C, the effect on the reduction rate is not significant, as it can be seen in Figs. 12 and 13, and at 1150 °C the reduction rates in the CO-CO<sub>2</sub> and H<sub>2</sub>-H<sub>2</sub>O-CO-CO<sub>2</sub> gases are equal, as seen in Fig. 13.

The higher reduction rates at 750 and 800 °C can be explained by the occurrence of the WGSR, which has its  $\Delta G = 0$  at 810 °C. Due to the WGSR, the gas probably contains more H<sub>2</sub>, which has a higher reduction potential than CO and thereby increases the rate of reduction. The WGSR is given in Eq. 8. The high amount of water vapour in the feed gas mixture (6.9 vol-%) at 750–900 °C prefers the WGSR to convert the gas towards equilibrium.

It has been shown that at high temperatures the WGSR has a high reaction rate and introducing a small quantity of H<sub>2</sub> into the gas mixture can produce remarkable effects on the reduction rate. The reducing time is cut significantly since H<sub>2</sub> accelerates the reduction process and the H<sub>2</sub>O produced reacts with CO to create H<sub>2</sub> which in turn takes part in the reduction again. It has been proposed that part of the H<sub>2</sub> does not participate in the reduction reaction but acts in a catalyst-like manner, which speeds up the reduction greatly. (Li *et al.* 2007, Ono-Nakazato *et al.* 2003).

At temperatures above 850 °C, reduction rates with H<sub>2</sub>-H<sub>2</sub>O-CO-CO<sub>2</sub> gas are not significantly higher than with CO-CO<sub>2</sub> mixtures which indicate that with equilibrated mixtures the 8 vol-% H<sub>2</sub>-H<sub>2</sub>O addition has no significant effect on the

reduction rate. The reverse WGSR above 850 °C can be also considered to explain the ineffectiveness of H<sub>2</sub> as if it reacts to form H<sub>2</sub>O at higher temperatures, it will not have increasing effect on the rate of reduction. According to Biswas (1981) the first 0–5% H<sub>2</sub> addition to CO should raise the reduction rate significantly in an atmosphere consisting purely of reductive gases, and the present experiment shows that such effect can be detected with CO-CO<sub>2</sub>-H<sub>2</sub>-H<sub>2</sub>O gas mixtures under the conditions used here at temperatures 750 and 800 °C, but not at temperatures above 850 °C.

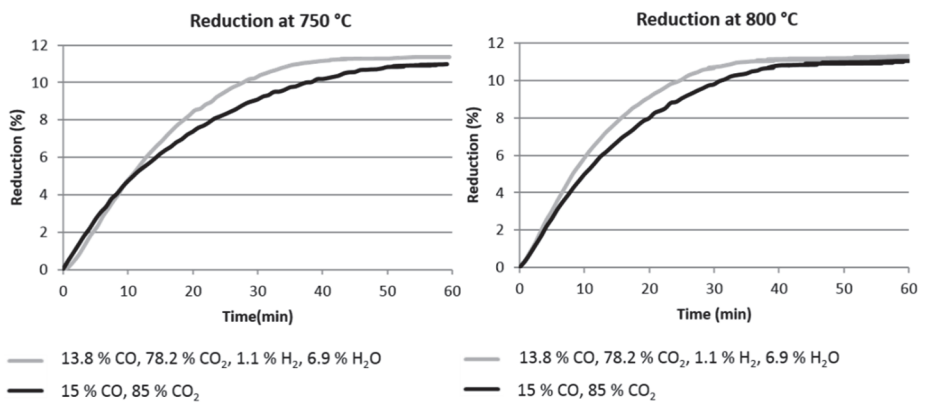


**Fig. 11. Reduction rate curves for pellets at 750 and 800 °C in CO-CO<sub>2</sub>-H<sub>2</sub>-H<sub>2</sub>O gas mixtures with a CO/CO<sub>2</sub> ratio of 15/85 (Paper I, reprinted by permission of ISIJ International).**

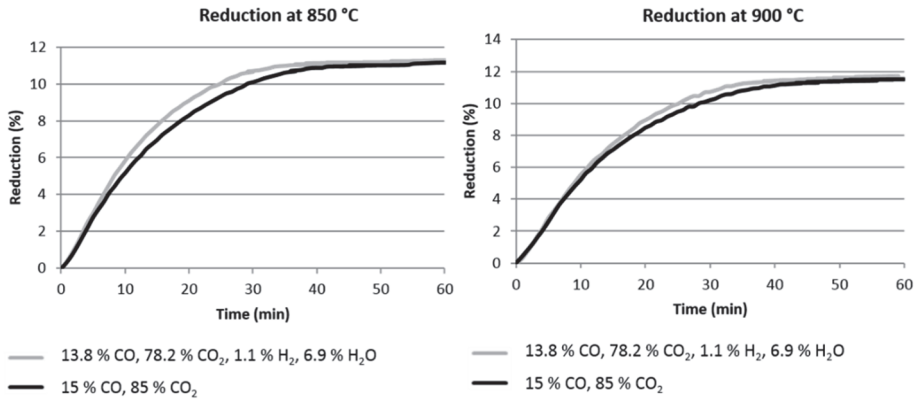


**Fig. 12.** Reduction rate curves for pellets at 850 and 900 °C in CO-CO<sub>2</sub>-H<sub>2</sub>-H<sub>2</sub>O gas mixtures with a CO/CO<sub>2</sub> ratio of 15/85 (Paper I, reprinted by permission of ISIJ International).

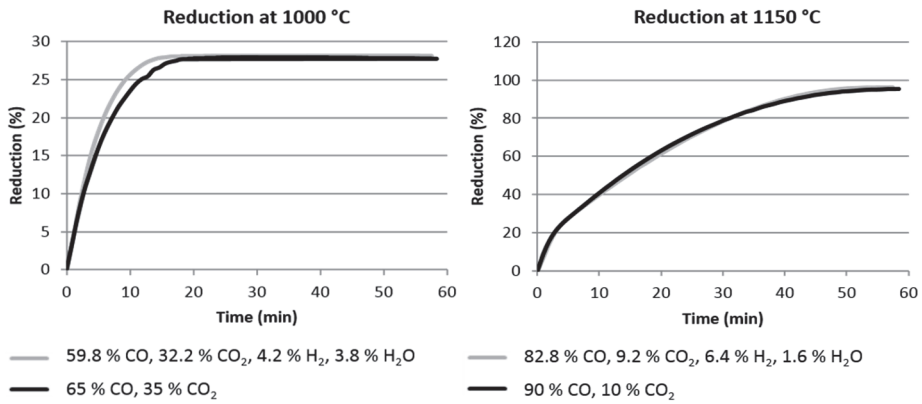


**Fig. 13.** Reduction rate curves for pellets at 1000–1150 °C in CO-CO<sub>2</sub>-H<sub>2</sub>-H<sub>2</sub>O gas mixtures with a CO/CO<sub>2</sub> ratios of 65/35 and 90/10 (Paper I, reprinted by permission of ISIJ International).

#### 4.1.2 Activation energy

In this work, activation energies were determined for CO-CO<sub>2</sub>-H<sub>2</sub>-H<sub>2</sub>O and CO-CO<sub>2</sub> gas mixtures for the hematite to magnetite reduction steps. Hematite to magnetite reduction reactions in CO and H<sub>2</sub> are given in Eqs. 1 and 2 respectively.

The reduction rate curves in Figs. 11 and 12 appear to be linear the first 4% of reduction. After 4% reduction the curves appear to change to non-linear, which indicates of change in the reaction mechanism. Therefore, slopes for the determination of apparent activation energies were obtained from 2% and 8% of reduction in the reduction rate curves shown in Figs. 11 and 12 to determine activation energies for both stages. The Arrhenius equation was used to determine the reaction rate constant. The reaction rate constant  $k$  can be expressed as an Arrhenius equation in the form of either Eq. 10 or Eq. 11 given below:

$$k = k_0 \cdot e^{-\frac{E_A}{R \cdot T}} \quad (10)$$

or

$$\ln k = -\frac{E_A}{R} \cdot \frac{1}{T} + \ln k_0 \quad (11)$$

where  $k_0$  is the frequency factor for the reaction,  $E_A$  the activation energy,  $R$  the universal gas constant (8.314 J×K<sup>-1</sup>×mol<sup>-1</sup>),  $T$  the temperature (K) and  $e$  Napier's constant (2.718).

Arrhenius plots obtained from calculated  $\ln(k)$  and  $1/T$  values at 2% and 8% reduction at temperature range 750–850 °C are shown in Fig. 14.

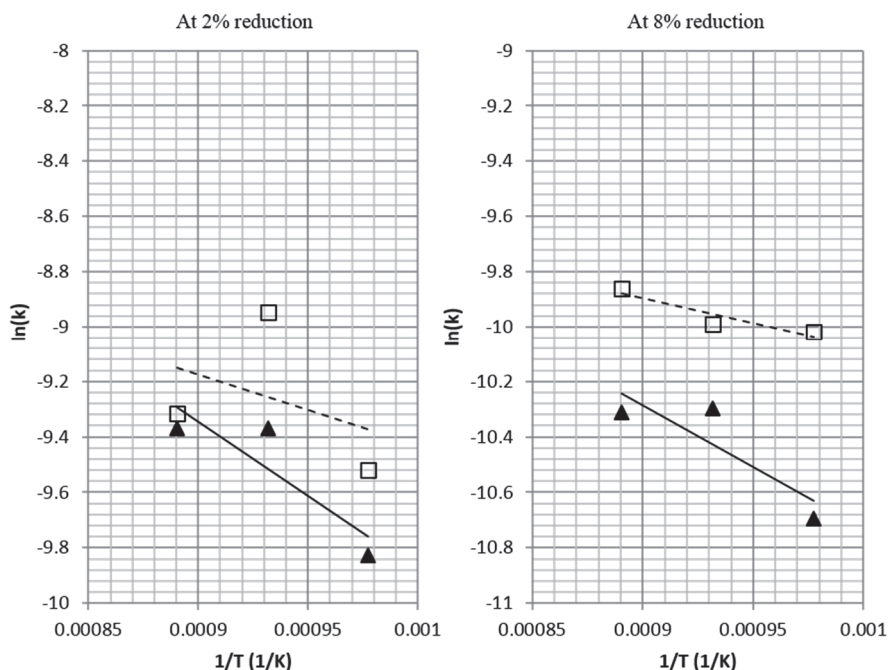


**Fig. 14. Apparent rate constant ( $k$ ) for the olivine pellets calculated from the tangent of the fraction of oxygen removed as a fraction of time at 2% reduction (left) and at 8% reduction (right) (Paper I, modified and reprinted by permission of ISIJ International).**

The apparent activation energies determined for the CO-CO<sub>2</sub> and H<sub>2</sub>-H<sub>2</sub>O-CO-CO<sub>2</sub> gases are shown in Table 8. The determined activation energies at 2% and 8% reduction are within the range of the values reported in the literature. The values for the activation energies of the initial stages in the reduction of iron oxides reported in the literature are shown in Table 9. Still, it must be noted that there are significant differences in the experimental conditions between these studies. For instance, Piotrowski *et al.* (2005) reduced a size of 91  $\mu\text{m}$  Fe<sub>2</sub>O<sub>3</sub> powder under a 30 ml/min gas flow rate, which differs considerably from the conditions used in the current experiments. El-Geassy (1986) reduced Fe<sub>2</sub>O<sub>3</sub> briquettes at a 1 l/min total gas flow rate and estimated the activation energies to be 56.5 kJ/mol for CO and 28.8 kJ/mol for H<sub>2</sub>-CO, which are near to the obtained values of this work.

At 2% reduction the activation energies of 44.39 kJ/mol determined for CO and 21.00 kJ/mol for H<sub>2</sub>-CO indicate higher reduction rate at initial reduction stage with H<sub>2</sub>-H<sub>2</sub>O addition. At 8% reduction determined activation energies of 37.21

kJ/mol for CO and 15.03 kJ/mol for H<sub>2</sub>-CO indicate also higher reduction rate with H<sub>2</sub>-H<sub>2</sub>O addition. The effect of an H<sub>2</sub> addition to the CO in lowering the activation energy shown in the literature was detected here at both 2% and 8% reduction stages.

**Table 8. Apparent activation energies ( $E_A$ ) determined for the CO-CO<sub>2</sub> and H<sub>2</sub>-H<sub>2</sub>O-CO-CO<sub>2</sub> gas mixtures at 2% and 8% reduction (kJ/mol) (Paper I, reprinted by permission of ISIJ International).**

Gas mixture	$E_A$ at 2% red.	$E_A$ at 8% red.
CO-CO <sub>2</sub>	44.39	37.21
H <sub>2</sub> -H <sub>2</sub> O-CO-CO <sub>2</sub>	21	15.03

**Table 9. Estimated activation energies reported in the literature for the initial stages in the reduction of iron oxides (Paper I, reprinted by permission of ISIJ International).**

Author	Reducing gas composition	$E_A$ (kJ/mol)
Piotrowski <i>et al.</i> (2005)	10% CO + 90% N <sub>2</sub>	104.1
El-Geassy (1986)	100% CO	56.5
Piotrowski <i>et al.</i> (2005)	10% H <sub>2</sub> + 90% N <sub>2</sub>	23.9
El-Geassy (1986)	100% H <sub>2</sub>	28.8
Piotrowski <i>et al.</i> (2005)	4.3% H <sub>2</sub> + 5.7% CO + 90% N <sub>2</sub>	79.6
El-Geassy (1986)	50% H <sub>2</sub> + 50% CO	40.1

#### 4.1.3 Sample microstructure

The sample microstructure investigation by FESEM revealed larger wüstite relics in the inner parts of the pellet sample reduced to iron in CO-CO<sub>2</sub> (exp. 6 in Table 5), but not in the pellet sample reduced to iron in H<sub>2</sub>-H<sub>2</sub>O-CO-CO<sub>2</sub> (exp. 12 in Table 5), as shown in LOM images in Fig. 15. Smaller wüstite relics and other phases were found in both these pellet samples as seen in the LOM images in Fig. 15. The observation indicates more efficient wüstite to iron reduction in H<sub>2</sub>-H<sub>2</sub>O-CO-CO<sub>2</sub> than in CO-CO<sub>2</sub> gas.

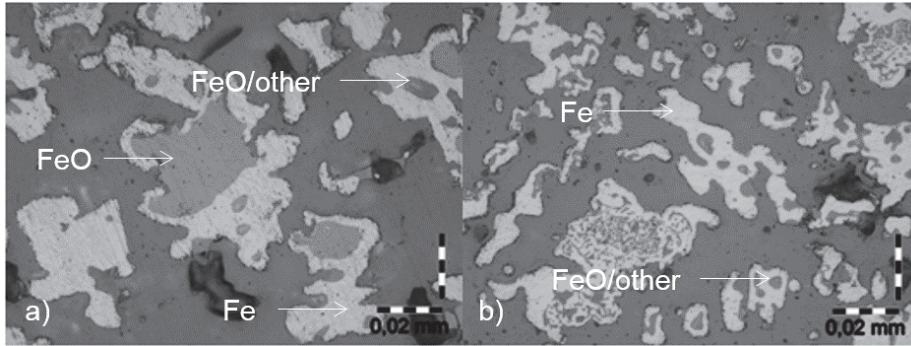


**Fig. 15.** Optical light microscope images of the pellets reduced to iron in CO-CO<sub>2</sub> ((a), exp. 6 in Table 5) and in H<sub>2</sub>-H<sub>2</sub>O-CO-CO<sub>2</sub> ((b), exp. 12 in Table 5) (Paper I, reprinted by permission of ISIJ International).

## 4.2 The effect of high H<sub>2</sub>O concentration in the BF shaft

The effect of the WGSR on the gas conversion in the conditions of upper part of BF shaft was investigated by LF experiments. The experimental conditions simulated high H<sub>2</sub>O concentration in CO-CO<sub>2</sub>-N<sub>2</sub> gas. The experimental conditions of the LF experiments are shown in Table 6 and Fig. 9.

Reactions occurring in the LF were investigated by analysing the gas samples taken from the GSPs 1–4 which are located at 0, 5, 10 and 15 cm heights from the bottom of the packed bed, respectively. The LF is illustrated in Fig. 8. Equilibrium concentrations of H<sub>2</sub> and CO gases were calculated by HSC Chemistry (Roine 2009). They were plotted in the figures together with the experimental gas analyses. The equilibrium constant ( $K_p$ ) of the WGSR was calculated with Eq. 12 and is plotted together with the experimental equilibrium constant values.

$$K_p = \frac{p_{CO_2} \times p_{H_2}}{p_{H_2O} \times p_{CO}} \quad (12)$$

where  $p_i$  = partial pressure of gas i. (atm)

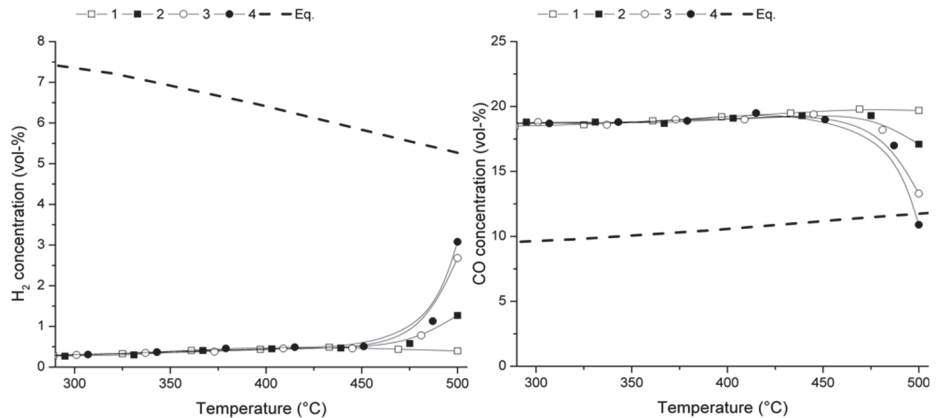
### 4.2.1 The WGSR in a hematite pellet layer

The reducing atmosphere was set to the phase stability area of magnetite in the Fe<sub>1-y</sub>O-Fe<sub>3</sub>O<sub>4</sub>-Fe<sub>2</sub>O<sub>3</sub> system with CO-CO<sub>2</sub>-H<sub>2</sub>O-N<sub>2</sub> gases in the HPL experiment (Fig. 9) because the catalysing effect of magnetite on the WGSR is known (Martos *et al.*

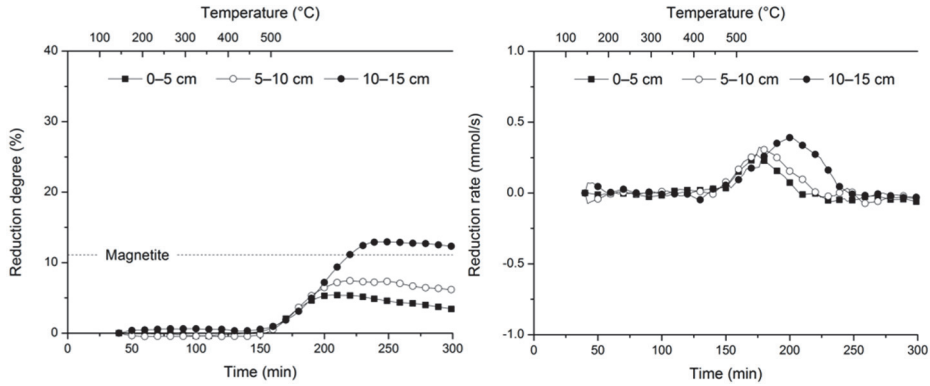
2009, Newsome 1980, Rhodes *et al.* 1995, Satterfield 1991, Smith *et al.* 2010). The conditions simulate the upper BF shaft area. For the experiment, the LF was filled (1.0 m layer) with hematite pellets (Low mag. olivine in Table 1). In the HPL experiment, the hematite pellets can be either reduced by CO or H<sub>2</sub>, if the WGSR takes place. The reduction reactions of hematite to magnetite in CO and H<sub>2</sub> are shown in Eqs. 1 and 2, respectively.

Fig. 16 shows that after reaching 450 °C, H<sub>2</sub> concentration increases indicating the WGSR in the pellet layer. H<sub>2</sub> increases first in GSP 4 and then in GSPs 3 and 2 reaching about 1–3 vol-% concentrations. In Fig. 16 it is possible to see that after reaching 450 °C, CO decreases first in GSP 4 and then in 3 and 2 for about 3–8 vol-%.

A higher conversion of CO compared to the formation of H<sub>2</sub> indicates that the reduction of hematite to magnetite also takes place at these temperatures. Thus, the reduction degree and reduction rate were determined in the HPL experiment and are shown in Fig. 17. A detailed description of the reduction degree and reduction rate calculation methods in the LF are presented in Paper II.



**Fig. 16. H<sub>2</sub> and CO concentrations in the LF filled with hematite pellets at 300–500 °C (Paper II, reprinted by permission of ISIJ International).**



**Fig. 17. Reduction degree and reduction rate of hematite pellets in HPL experiment (Paper II, reprinted by permission of ISIJ International).**

Reduction degree curves in Fig. 17 indicate the pellet layers of 0–5, 5–10 and 10–15 cm have reached the hematite to magnetite reduction degree after about 200, 220 and 240 minutes, respectively. The same observation can be made in the reduction rate curves. According to Fig. 17, the reduction degree and reduction rate are highest in the pellet layer at 10–15 cm height. The equilibrium constant of the WGS at 300–500 °C shows that experimental gas converts towards equilibrium as it can be seen in Fig. 18. It should be noticed that experimental gas composition is here affected by the reduction and the WGS.

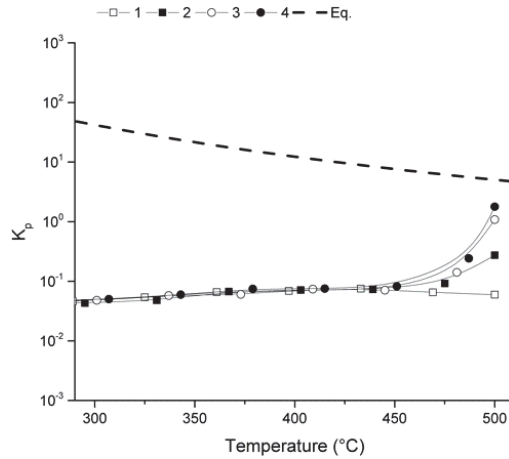


**Fig. 18. Equilibrium constant of the WGS in HPL experiment at 300–500 °C (Paper II, reprinted by permission of ISIJ International).**

After reaching 500 °C, the temperature was held constant for 150 min in order to investigate the gas conversion towards the theoretical equilibrium composition at 500 °C. H<sub>2</sub> and CO concentrations, shown in Fig. 19, reach a steady state after 75 min in each GSP, indicating the end of the hematite to magnetite reduction. During the period between 75 and 150 min 4–6 vol-%, H<sub>2</sub> is formed and CO concentration decreases correspondingly 4–6 vol-%. Thus, CO conversion between 75–150 min can be considered to be caused solely by the WGS. Fig. 20 shows that the gas composition reaches theoretical equilibrium at 500 °C after the hematite to magnetite reduction in the GSP 4 and almost in the GSPs 3 and 2.

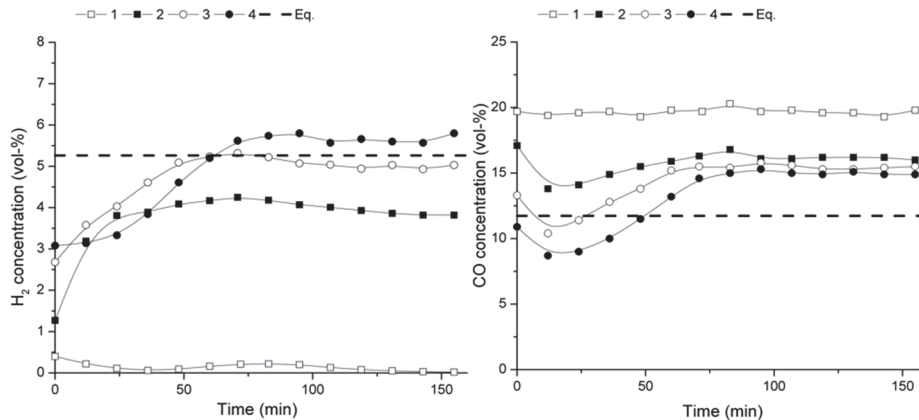


Fig. 19. H<sub>2</sub> and CO concentration in the LF filled with hematite pellets at 500 °C (Paper II, reprinted by permission of ISIJ International).

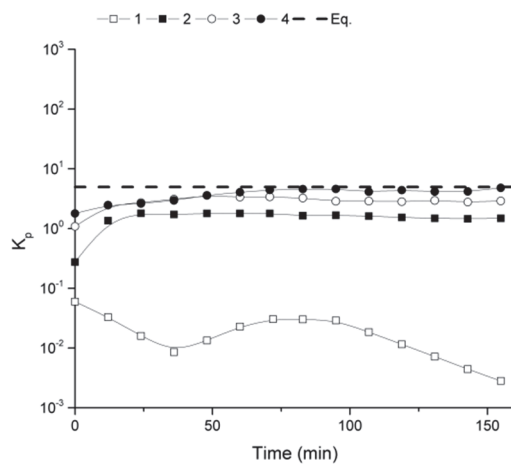


Fig. 20. Equilibrium constant of the WGS in HPL experiment at 500 °C (Paper II, reprinted by permission of ISIJ International).

#### 4.2.2 The WGSR in a magnetite pellet layer

The catalysing effect of magnetite on the WGSR was investigated further with an experiment where olivine pellets pre-reduced to magnetite were used. The pre-reduction procedure is described in Paper II. The feed gas and the temperature profile in the MPL experiment were identical to the HPL experiment. An increase of H<sub>2</sub> concentration and decrease of CO shown in Fig. 21 indicate the WGSR at the temperature range from 300 to 400 °C. At first, H<sub>2</sub> increases in GSP 4 at above 300 °C. The WGSR is observed at slightly higher temperatures in the lower GSPs. According to the equilibrium constant in Fig. 22, the gas converts towards the equilibrium at 300–500 °C. The catalysing effect of magnetite can be seen when these observations are compared to the results of HPL experiment. During the time LF was held at 500 °C, H<sub>2</sub> and CO concentrations showed constant values, which can be seen in Fig. 23. This indicates the occurrence of the WGSR and the H<sub>2</sub> concentration is near to the thermodynamic equilibrium composition at 500 °C in GSPs 3 and 4. The gas converts to the equilibrium composition rapidly in the magnetite pellet layer at 500 °C as shown in Fig. 24. Reduction reactions of iron oxides were not detected in the experiment.

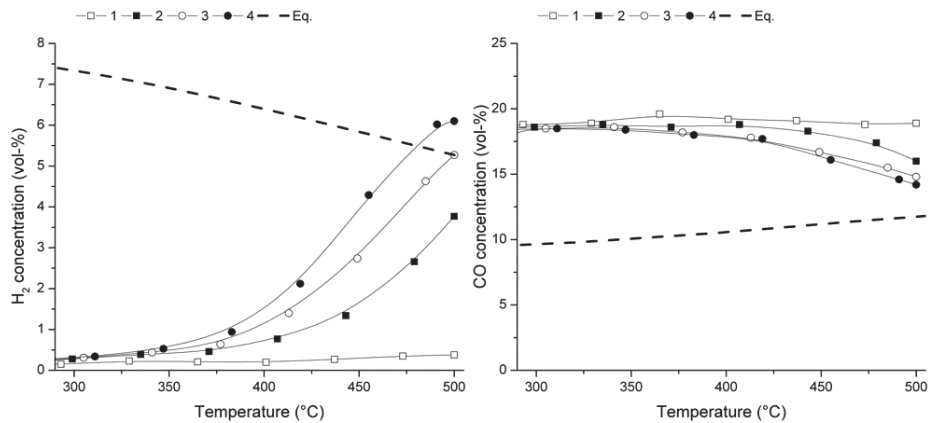


Fig. 21. H<sub>2</sub> and CO concentration in the LF filled with magnetite pellets at 300–500 °C (Paper II, reprinted by permission of ISIJ International).

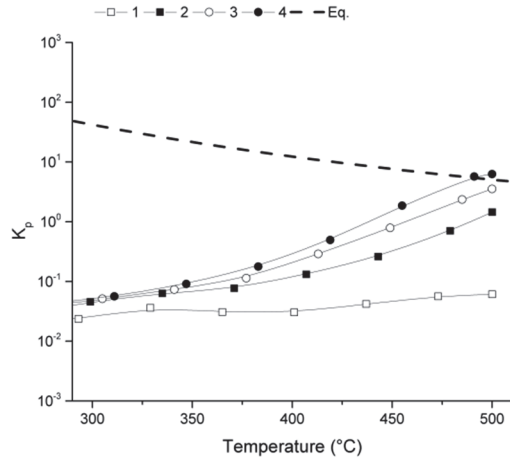


Fig. 22. Equilibrium constant of the WGSR in MPL experiment at 300–500 °C (Paper II, reprinted by permission of ISIJ International).

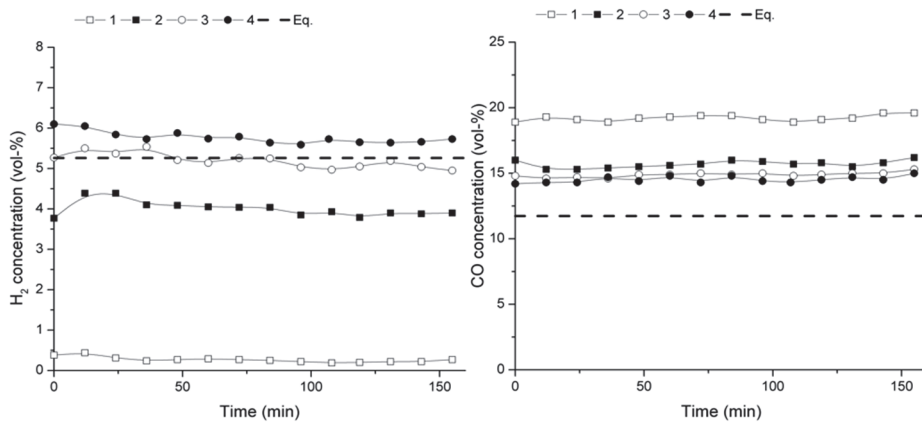
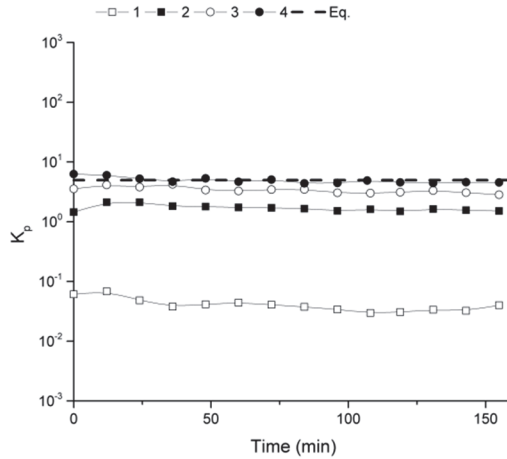


Fig. 23. H<sub>2</sub> and CO concentration in the LF filled with magnetite pellets at 500 °C (Paper II, reprinted by permission of ISIJ International).



**Fig. 24. Equilibrium constant of the WGSR in MPL experiment at 500 °C (Paper II, reprinted by permission of ISIJ International).**

#### **4.2.3 Reaction rate of the WGSR**

The reaction rate of the WGSR was estimated by calculating the formation rate of H<sub>2</sub> in the HPL and MPL experiments. It must be noted that the formation rate of H<sub>2</sub> is affected by both the reduction and the WGSR, in opposite directions. Further, the H<sub>2</sub> formation rate depicts the reaction rate of the WGSR when no reduction of iron oxides occurs. A detailed calculation method for the reaction rate is presented in Paper II.

The formation rates of H<sub>2</sub> in the HPL and MPL experiments are shown in Fig. 25. It was seen in the HPL experiment that the reduction of hematite ends after about 240 min and Fig. 25 shows constant formation rates of H<sub>2</sub> after that as well. The formation rates of H<sub>2</sub> in the MPL experiment show steady values after 200 min. In Fig. 25 it can be seen that the formation rate of H<sub>2</sub> is the highest in the lowest 5 cm part of the pellet layer and shows lower values in the higher layers. This suggests that the gas converts rapidly towards the equilibrium in the lowest 5 cm part of the pellet layer. It should be noted, however, that no reduction reactions occurred in the MPL experiment, and therefore the H<sub>2</sub> formation rate illustrates solely the rate of the WGSR.

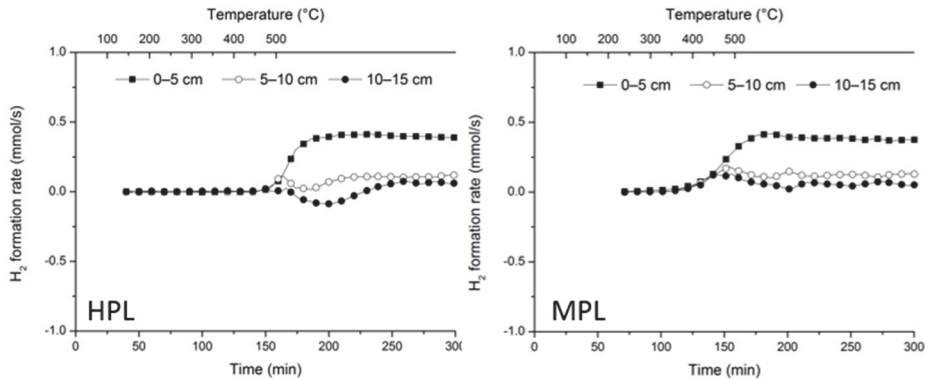


**Fig. 25. Reaction rate of the WGSR in HPL and MPL experiments (Paper II, modified and reprinted by permission of ISIJ International).**

### 4.3 Reduction behaviour of cold-bonded briquette

In this study, the briquettes were reduced by BFS under a dynamic reduction programme, which has been previously used to study the reduction behaviour of iron ore pellets (Iljana *et al.* 2012, Iljana *et al.* 2013). The aim was to study the reduction rate, swelling and phase transformations in the briquettes when the iron oxides are reduced to magnetite, wüstite and iron in the BFS (Figs. 6–7). Additionally, the effect of the GGBFS on the reduction behaviour was investigated with samples where GGBFS was used as a cement replacement (Table 3). The reduction of the cold-bonded briquette was compared to the olivine fluxed iron ore pellet which was used as a reference sample (Table 1).

#### 4.3.1 Phase transformations

The XRD peaks for the briquette sample 0 are shown in Fig. 26. The XRD peaks show the phase transformations in the cold-bonded briquette during the reduction. Only the peaks of the sample with PC binder (Sample 0, Table 4) are presented because very few differences were detected between the XRD analyses of the briquette samples. More details about the conducted XRD analyses are presented in Paper III.

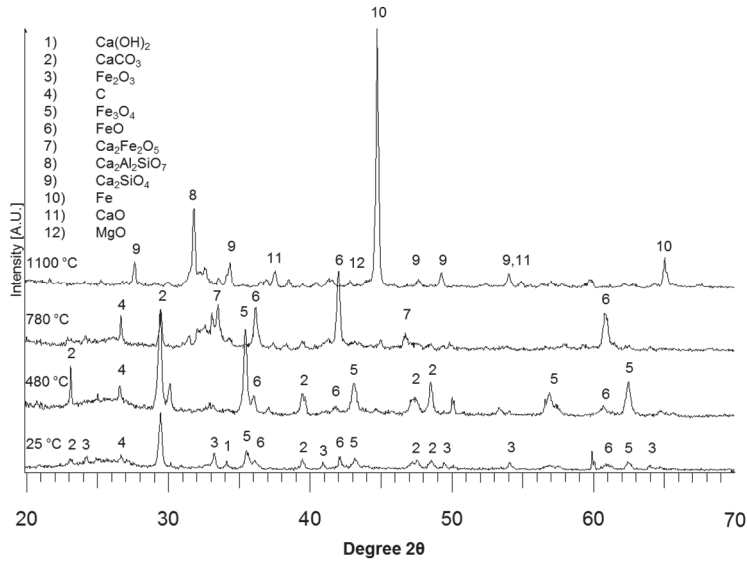
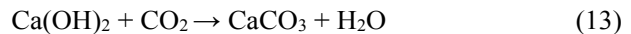


**Fig. 26. XRD analysis of the briquette sample 0 at 25, 480, 780 and 1100 °C temperatures (Paper III, reprinted by permission of ISIJ International).**

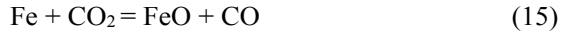
#### *Phase stability area of magnetite at 480 °C*

Raw briquette samples consist mainly of divalent ( $\text{Fe}^{2+}$ ) and trivalent ( $\text{Fe}^{3+}$ ) iron oxides, portlandite ( $\text{Ca}(\text{OH})_2$ ), carbon (C) and calcium carbonate ( $\text{CaCO}_3$ ) at room temperature as shown in Fig. 26. Raw samples also contain larger particles of metallic iron (Fe), which is not shown in the XRD because of the sample preparation, for which they could not be ground to a fine particle size.

In the conditions of the “Magnetite” experiment hematite and portlandite have disappeared from the briquette sample at temperatures below 480 °C and the peaks of magnetite and calcium carbonate have increased as shown in Fig. 26. The hematite to magnetite reduction takes place according to Eq. 1. In the presence of  $\text{CO}_2$ , calcium carbonate is formed from the portlandite according to Eq. 13. The released water vapour may have an effect on the reduction of iron oxides through the water-gas shift or the water-gas reactions which are given in Eqs. 8 and 14, respectively.

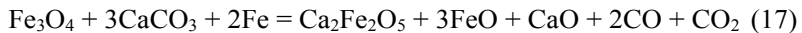


In addition to the hematite to magnetite reduction, the metallic iron in the briquette may be oxidised either by Eq. 15 or Eq. 16. Reduction causes weight loss and oxidation increases the weight of the sample.



### *Phase stability area of wüstite at 780 °C*

The XRD peaks in Fig. 26 show that magnetite is reduced to wüstite in the samples at 780 °C. The magnetite to wüstite reduction in CO is given in Eq. 3. In the “Wüstite” experiment, the di-calcium ferrite ( $\text{Ca}_2\text{Fe}_2\text{O}_5$ ) phase has appeared in the briquette sample, whereas peaks of calcium carbonates have decreased. At 780 °C, the amount of calcium carbonate phase has decreased in comparison to the lower temperature, whereas the di-calcium ferrite phase has appeared in the briquette samples according to the XRD peaks presented in Fig. 26. This indicates that part of the calcium carbonate has decomposed and formed di-calcium ferrite together with the iron oxides in a complex series of reactions shown in Eq. 17. According to Robinson *et al.* (2005) this reaction series occurs approximately at 750 °C. The di-calcium ferrite phase is a stable phase under the conditions of “Wüstite” experiment which is pointed out in Paper III.



### *Phase stability area of iron at 1100 °C*

In “Iron 1” and “Iron 2” experiments, divalent iron is reduced to metallic iron according to Eq. 5. Fig. 26 shows that in “Iron 1” and “Iron 2” experiments at 1100 °C, carbon, the calcium carbonate and di-calcium ferrite phases have disappeared. Carbon has gasified and calcium carbonate and di-calcium ferrite have decomposed through thermal decomposition and reduction, respectively. All iron is reduced to metallic and the samples contain some larnite ( $\text{Ca}_2\text{SiO}_4$ ), gehlenite ( $\text{Ca}_2\text{Al}_2\text{SiO}_7$ ), iron (Fe), lime (CaO) and periclase (MgO). According to the phase stability systems of Schuermann and Wurm (1973), metallic iron and lime are the stable phases at the conditions of “Iron 1” and “Iron 2” experiments which is shown in Paper III. In the briquettes, the remaining calcium carbonates have decomposed through the thermal decomposition by Eq. 18 at around 840 °C. The di-calcium ferrite phase ( $\text{Ca}_2\text{Fe}_2\text{O}_5$ ) has been reduced to Fe and CaO by Eq. 19 at about 950 °C.



### 4.3.2 Reduction and swelling

The weight losses of the samples in the experiments are shown in Fig. 27. A slight reduction of iron oxides occurred in the “Magnetite” experiment since the reference pellet lost about 1% of its weight as seen in Fig. 27. Weight loss of the pellet indicates approximately 3.1% RD, whereas the calculated complete RD of magnetite would be approximately 11.6%.

Fig. 27 shows weight losses of about 5–6% for all the samples and slightly higher weight losses on the briquette samples (+ 0.5–1%) than on the pellet in the “Wüstite” experiment. The weight loss of the reference pellet indicates about 18% RD, when the calculated complete RD of wüstite would be about 33%.

The weight losses of the briquette samples are from 27 to 31% in the “Iron 1” and “Iron 2” experiments as can be seen in Fig. 27. It is notable that weight losses of briquette samples in “Iron 1” and “Iron 2” experiments are equal, which indicates 100% RD already in the “Iron 1” for the briquette samples. The weight losses of the pellets are 22% and 27% in “Iron 1” and “Iron 2” which indicate RDs of 75.5% and 92%, respectively. The effect of the 60 min time extension in “Iron 2” leads to markedly higher RD with the pellet. The higher reduction degree of the briquette in “Iron 1” is probably achieved by the self-reducing effect of the carbon which reacts according to the Boudouard reaction (Eq. 20). The CO formed in the Boudouard increases the reduction rate of the briquette.



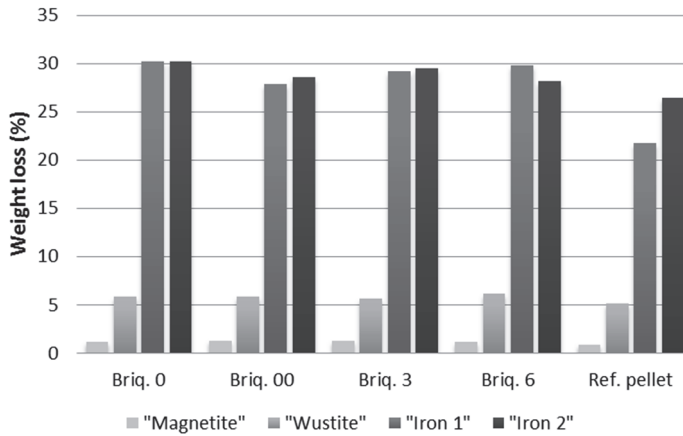


**Fig. 27. Weight losses (%) of the briquette and pellet samples in the experiments (Paper III, reprinted by permission of ISIJ International).**

The swelling (vol-%) of the samples are shown in Fig. 28. The 0 sample was introduced twice in the experiments and these samples are labelled as 0 and 00 in the figures. Fig. 29 shows video camera images of the swelling of the briquettes. These images show that the swelling of the briquettes takes place during the wüstite-iron reduction step at 900–1000 °C. The original work shows that the structure of the briquette sample is considerably more porous when reduced to iron in comparison to other experiments (Paper III).

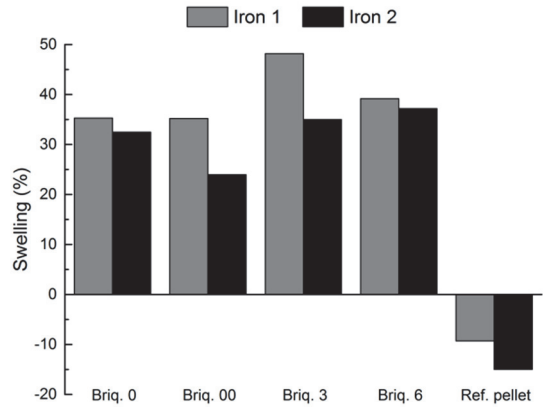


**Fig. 28. Swelling (vol-%) of the briquette and pellet samples in “Iron 1” and “Iron 2” experiments (Paper III, reprinted by permission of ISIJ International).**

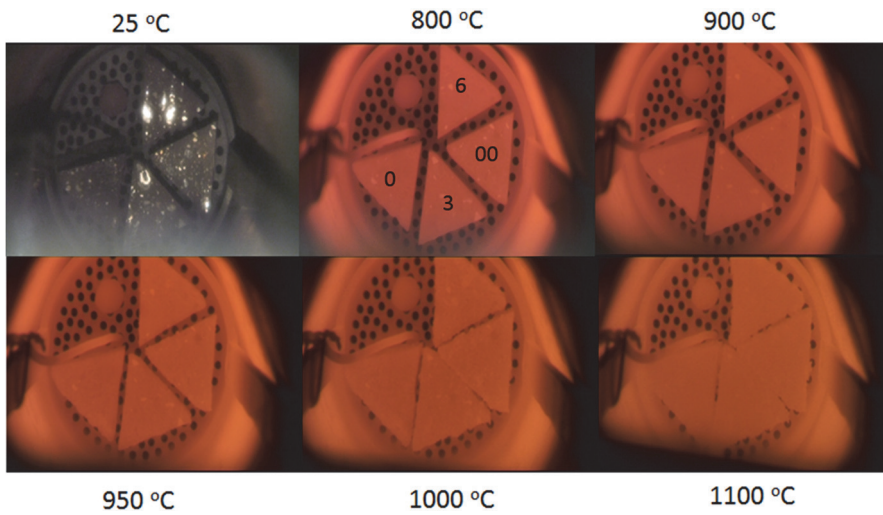


**Fig. 29. Images of sample basket captured from “Iron 1” experiment at 25–1100 °C (Paper III, reprinted by permission of ISIJ International).**

#### 4.4 Softening behaviour of iron ore pellet

The softening behaviours of acid and olivine fluxed iron ore pellets (Table 1) in the cohesive zone of the BF were investigated using the CZS equipment. The iron ore pellets were previously pre-reduced to RDs of 50–70% by the BFS, which has been used to study the reduction behaviour of iron ore pellets and cold-bonded briquettes (Iljana *et al.* 2012, Kemppainen *et al.* 2014). The pellet pre-reduction procedure is presented in Paper IV. The contraction-% of the pellet was calculated from the measured displacement (mm) in a vertical direction during the softening experiments. Microstructural analysis of the samples was carried out to find out the mechanism causing the softening in both cases. The phase evolution in the pellets was investigated by computed phase diagrams.

##### 4.4.1 Contraction

In Fig. 30, the contraction-% curves of the acid pellets are shown. The softening starts at around 1100 °C and the pellets soften rapidly at 1150 °C. The contraction-% curves of pellets pre-reduced to 50, 60 and 70% have no significant differences. The pellet with the highest RD (70%) appears to reach the rapid softening stage slightly faster. The pellet with the lowest RD (50%) reaches its highest contraction-% at 1200 °C.

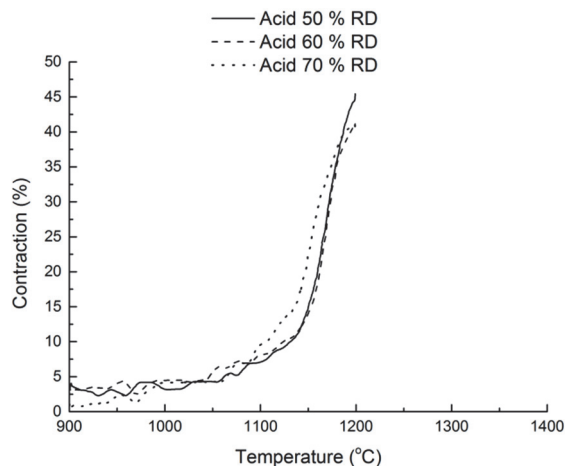
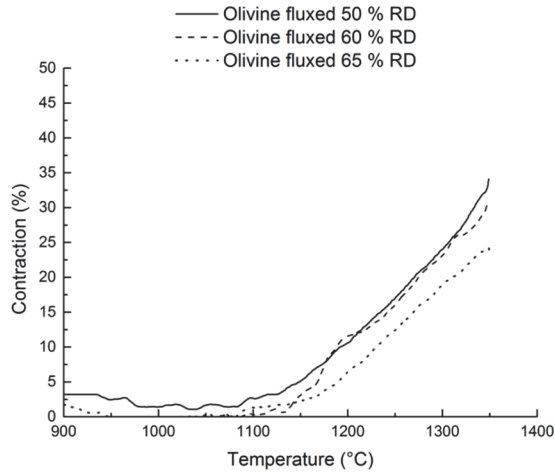


Fig. 30. Contraction-% curves of the acid pellets in the softening experiments (Paper IV, reprinted by permission of ISIJ International).

The contraction-% curves of the olivine fluxed pellets in Fig. 31 show that they begin to soften at around 1150 °C. The rate of softening of the olivine fluxed pellet appears to be constant up to a temperature of 1350 °C. The pellet with the highest RD (65%) displays slightly slower softening compared to the RDs of 50 and 60%. The pellet with the lowest RD (50%) has the highest contraction-% at 1350 °C.



**Fig. 31. Contraction-% curves of the olivine fluxed pellets in the softening experiments (Paper IV, reprinted by permission of ISIJ International).**

#### **4.4.2 Phase evolution**

The cause for different softening behaviour of acid and olivine fluxed pellet was sought from the microstructures of the pellets. The phase evolutions in the pre-reduced and softened acid and olivine fluxed pellets were investigated by LOM and FESEM-EDS analyses. FactSage V6.4 -software and its FToxid-database was used to compute the phase equilibrium of a pre-reduced pellet with a quaternary FeO-SiO<sub>2</sub>-CaO-MgO system (Bale *et al.* 2013). The phase evolution which was analysed from the pellet microstructure was compared to the computed phase system.

### *The acid pellet*

The LOM images of the periphery part and the core part in the pre-reduced (1100 °C) acid pellet (RD = 60%) are shown in Fig. 32. The periphery area of the pellet is highly porous and mostly consists of metallic iron ( $\text{Fe}^0$ ) and a fayalite ( $\text{Fe}_2\text{SiO}_4$ ) slag phase. The core of the pre-reduced pellet has a porous structure and it mainly consist of wüstite and the fayalite slag phase. The wüstite particles are connected to each other forming a partly uniform structure. The slag phase surrounds the wüstite. Some small phases of metallic iron are found in the core.

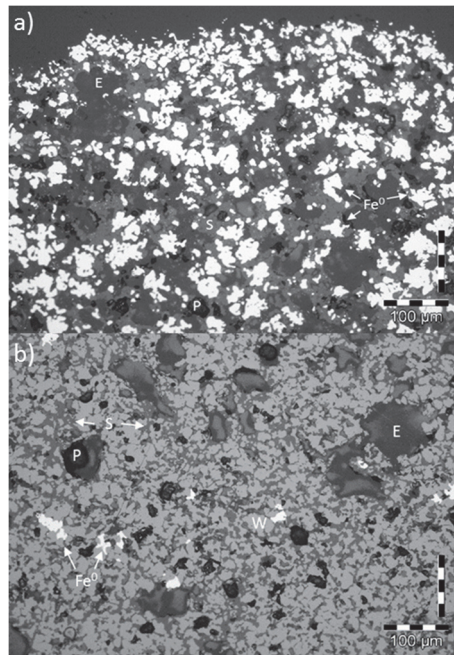


**Fig. 32.** The LOM images of the periphery part (a) and the core part (b) in the pre-reduced (1100 °C) acid pellet (RD = 60%); E = epoxy, S = slag (fayalite),  $\text{Fe}^0$  = metallic iron, P = pore, W = wüstite (Paper IV, reprinted by permission of ISIJ International).

The LOM images of the periphery part and the core part of the softened acid pellet (1200 °C) are shown in Fig. 33. In the softened acid pellet, the wüstite phase can be seen to be separated from each other and its particle size is smaller than 50  $\mu\text{m}$ . The wüstite particles are surrounded by the slag phase. The amount of the fayalite slag is higher in the periphery area. The FESEM analyses of the acid pellet samples

indicate that the wüstite phase is mostly pure and the fayalite slag phase contains approximately 0.5–2 wt-% CaO and 0.5–1.5 wt-% MgO as dissolved components. No significant differences were detected between FESEM analyses of pre-reduced (1100 °C) and softened (1200 °C) acid pellet samples.

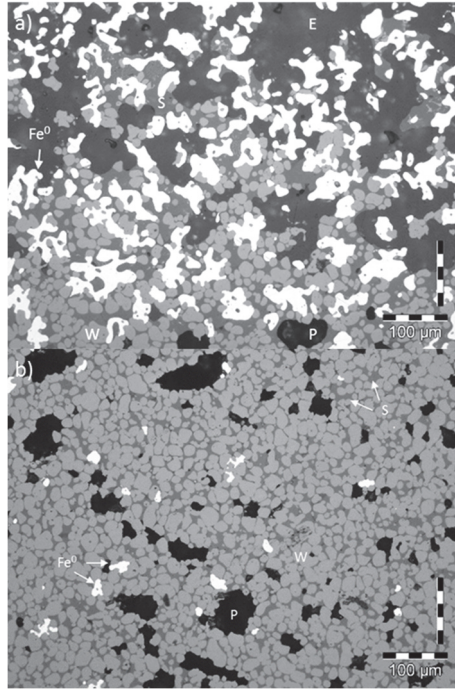


**Fig. 33. The LOM images of the periphery part (a) and the core part (b) in the pre-reduced (1200 °C) acid pellet (RD = 60%); E = epoxy, S = slag (fayalite), Fe<sup>0</sup> = metallic iron, P = pore, W = wüstite (Paper IV, reprinted by permission of ISIJ International).**

In Fig. 34 is shown a FactSage computed FeO-SiO<sub>2</sub>-CaO-MgO diagram with the composition of the acid pellet illustrated with dashed black line (5.27 wt-% SiO<sub>2</sub> content) in the FeO-SiO<sub>2</sub>-CaO-MgO system (0.5 wt-% CaO and 0.15 wt-% MgO). The phase diagram shows that the first forming liquid slag phase has an approximate solidus temperature of 1162 °C. Between 1162 and 1187 °C the fayalite slag melts and the olivine phase dissolves as seen in Fig. 34. The FactSage computed liquid oxide phase fraction-% of the acid pellet is shown in Fig. 35. The liquid oxide phase fraction-% increases rapidly above 1162 °C up to 20% as seen

in Fig. 35. This indicates high wüstite dissolution in the slag phase. Above 1187 °C the slag is coexisting with the magnesiowüstite as seen in Fig. 34. The FESEM analyses indicated mostly pure wüstite in the core part of the acid pellet. Fig. 35 shows that between 1187 and 1300 °C the share of the liquid slag phase increases slightly as the magnesiowüstite dissolves in it. Above 1300 °C the liquid slag fraction-% increases rapidly again and the system reaches its liquidus at 1348 °C.

The acid pellet softened rapidly at 1150 °C in the experiments near the solidus temperature (1162 °C) of the slag phase. A small amount of alkalis probably have a slight decreasing effect on the solidus and liquidus temperatures, which would explain the difference in the softening and the slag solidus temperatures. The most significant visible structural change between the pre-reduced pellet (1100 °C) and the softened one (1200 °C) is the transformation of wüstite into separate particles a size less than 50 µm surrounded by the slag phase as seen in Fig. 33. This indicates the formation of a slag phase with a high wüstite solubility. The results showed that reaching the solidus temperature of the acid pellet has a crucial effect on the softening because it will cause formation of molten fayalite slag where the wüstite dissolves in large amounts. The single wüstite particles (<50 µm) surrounded by the slag cannot resist the deformation of the pellet under pressure. The rapid softening of the acid pellet led to a contraction of 40% at 1200 °C in the experiments. If the computed quaternary FeO-SiO<sub>2</sub>-CaO-MgO diagram is compared to a phase diagram of a pure FeO-SiO<sub>2</sub> system it can be seen that the fluxes (CaO) decrease the temperature in which the first melt is formed. The first slag forms in the current FeO-SiO<sub>2</sub> system at 1162 °C as shown in Fig. 34 and in the pure FeO-SiO<sub>2</sub> system with 5.27 wt-% SiO<sub>2</sub> approximately at 1190 °C (Atlas 1995).

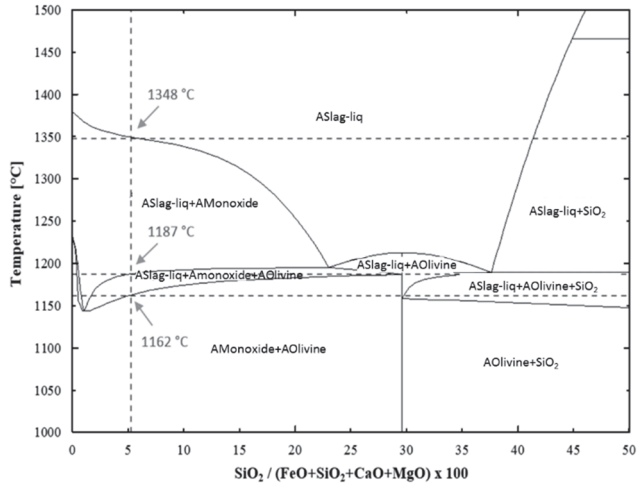


Fig. 34. A FactSage computed FeO-SiO<sub>2</sub>-CaO-MgO diagram with the composition of the acid pellet marked with a dashed vertical line; AMonoxide = (Fe,Mg)O, AOlivine = (Fe,Mg,Ca)<sub>2</sub>SiO<sub>4</sub> (Paper IV, reprinted by permission of ISIJ International).

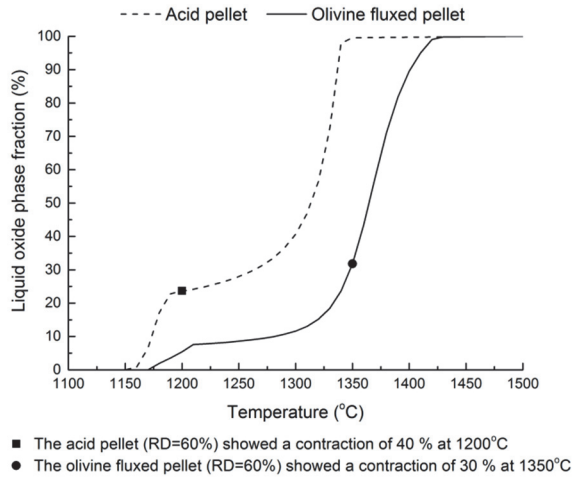
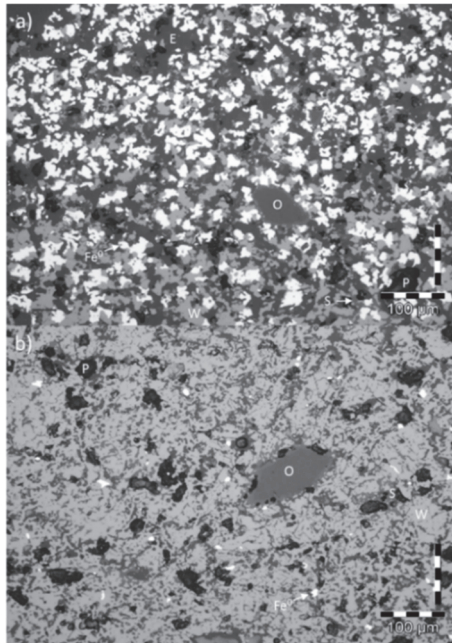


Fig. 35. A FactSage computed evolution of liquid oxide phase as a function of temperature (Paper IV, reprinted by permission of ISIJ International).

### *The olivine fluxed pellet*

The LOM images of the periphery part and the core part in the pre-reduced (1100 °C) olivine fluxed pellet (RD = 60%) are shown in Fig. 36. The FESEM-EDS was used to identify the phases. The highly porous periphery area consists mainly of metallic iron, wüstite and a fayalite slag phase. Olivine grains are undissolved in the structure of the pre-reduced pellet. The core of the pellet consists of wüstite as a major uniform phase and a minor slag phase. Small metallic iron phases are found in the core of the pellet as seen in Fig. 36.



**Fig. 36.** The LOM images of the periphery part (a) and the core part (b) in the pre-reduced (1100 °C) olivine fluxed pellet (RD = 60%); E = epoxy, S = slag (fayalite), Fe<sup>0</sup> = metallic iron, P = pore, W = wüstite, O = olivine (Paper IV, reprinted by permission of ISIJ International).

The porous periphery area of the softened (1350 °C) olivine fluxed pellet consists of metallic iron and wüstite surrounded by the fayalite slag phase as seen in Fig. 37. The core of the pellet consists of round wüstite particles surrounded by the slag. The size of the wüstite particles is approximately 50–100 μm. The amount of slag

phase is higher in the periphery than in the core. The core of the pellet is highly porous. The fayalite phase contains approximately 4 wt-% dissolved MgO and 5 wt-% CaO in the core of the pellet. The wüstite phase has about 1 wt-% dissolved MgO. The concentrations of dissolved components are higher in the periphery area where porosity is higher and less wüstite is present.

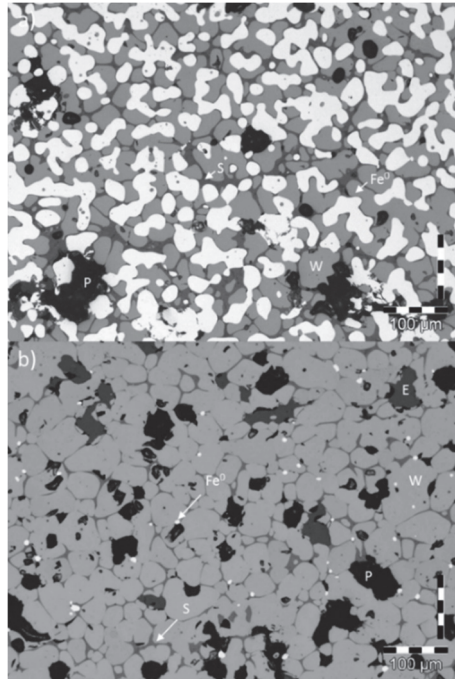


**Fig. 37. The LOM images of the periphery part (a) and the core part (b) in the pre-reduced (1350 °C) olivine fluxed pellet (RD = 60%); E = epoxy, S = slag (fayalite), Fe<sup>0</sup> = metallic iron, P = pore, W = wüstite (Paper IV, reprinted by permission of ISIJ International).**

The pre-reduced (1100 °C) olivine fluxed pellet consists of metallic iron, wüstite, olivine grains and fayalite slag phase. The olivine grains are undissolved at 1100 °C as shown in Fig. 36. A FactSage diagram in Fig. 38 shows that the slag phase has a solidus temperature at 1169 °C. The meltdown of fayalite phase and dissolution of the olivine phase takes place in the range of 1169–1205 °C where the liquid slag fraction increases up to 5% as seen in Fig. 35. Dissolution of olivine grains release MgO which dissolves into the fayalite slag phase and the wüstite phase increasing their solidus and liquidus temperatures. The effect of MgO on the phase system can

be seen in Fig. 38. In the range of 1205–1310 °C the liquid slag fraction-% increases slowly as the dissolution of the magnesiowüstite in the slag takes place. Above 1310 °C the rate of the liquid slag formation increases and the phase system has liquidus at 1427 °C.

In the present experiments, the olivine fluxed pellet started to soften at 1150 °C and kept softening gradually up to 1350 °C. Rapid softening was not seen when the solidus temperature of the first liquid slag phase was reached. This observation indicates that the wüstite will not dissolve in large amounts in the slag phase to form low melting point fayalite. Fig. 35 shows that the liquid slag fraction-% remain markedly lower in the olivine fluxed pellet than in the acid pellet. The computed liquid slag fraction-% of the olivine pellet exceeds 20% at 1340 °C which led to contraction of 30–35% in the experiments. This correlates reasonably with the contraction of the acid pellet at 1200 °C (40% contraction) with a liquid slag fraction higher than 20%. The size of the wüstite particles surrounded by the slag is about 50–100 μm at 1350 °C. The gradual softening of the olivine pellet can be attributed to the lower SiO<sub>2</sub> quantity of the slag phase and on the effect of fluxes (MgO, CaO).

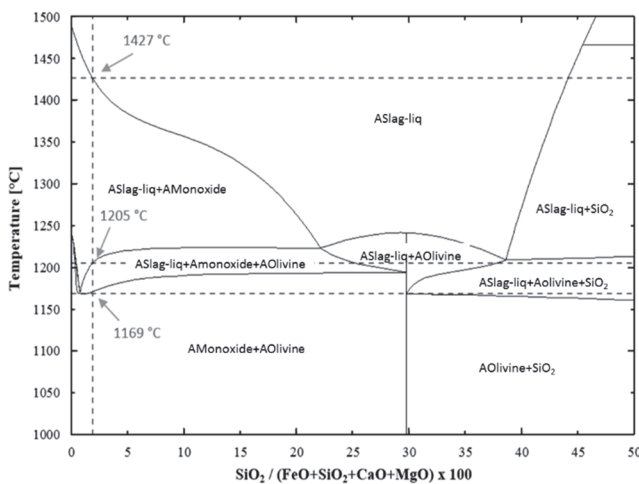


**Fig. 38. A FactSage computed FeO-SiO<sub>2</sub>-CaO-MgO diagram with the composition of the olivine fluxed pellet marked with a dashed vertical line; AMonoxide = (Fe,Mg)O, AOlivine = (Fe,Mg,Ca)<sub>2</sub>SiO<sub>4</sub> (Paper IV, reprinted by permission of ISIJ International).**



## 5 Discussion

### 5.1 Iron oxide reduction in H<sub>2</sub>-H<sub>2</sub>O-CO-CO<sub>2</sub> gas

In this thesis, the effect of the H<sub>2</sub> on the iron oxide reduction was studied with equilibrated H<sub>2</sub>-H<sub>2</sub>O-CO-CO<sub>2</sub> gases. In the literature, the effect of H<sub>2</sub> is typically tested with pure CO and H<sub>2</sub> gases. According to El-Geassy *et al.* (1977), the lower reduction rate of iron oxides in pure CO than in pure H<sub>2</sub> may be due to the much lower diffusivity of CO and the probability of blockage by carbon deposited in the pores of the initially formed solid iron ( $2\text{CO} = \text{CO}_2 + \text{C}$ ). Pure hydrogen is a superior reducing agent at first, but later, at a high degree of reduction, the rate slows down. In the case of CO, although the rate is sluggish initially, the last portion of the oxygen is removed more quickly. The longer time taken by hydrogen for complete reduction is probably due to the formation of a dense non-porous iron shell. Much quicker reduction than that obtained either with H<sub>2</sub> or with CO can be effected if both of them are present in the reducing gas. This is due to the carburizing effect of the CO gas on the iron. The carbon diffuses to the wüstite/iron interface, reacts to form CO + CO<sub>2</sub> and a high gas over-pressure is built up inside which breaks the surrounding iron film, thus permitting further gas exchange at the oxide/metal interface. In the case of hydrogen only, the steam over-pressure is not sufficient to burst the shell open. With a CO-H<sub>2</sub> gas mixture, however, the CO performs the bursting, opening up the passage for hydrogen with its greater reducing power.

Ke-qin & Jia-xin (1993) proposed that a 0–5% H<sub>2</sub> addition to CO will increase the degree of reduction significantly (a 2–5% increase for each 1% H<sub>2</sub>), but that a further 5% will give much less improvement (1% for each 1% of additional H<sub>2</sub>). El-Geassy (1986) detected a significant increase in the rate of reduction in the initial stages when reducing Fe<sub>2</sub>O<sub>3</sub> compacts from 600 to 1050 °C in a gas mixture consisting of 25% H<sub>2</sub> and 75% CO. He found that the addition of CO to an H<sub>2</sub> atmosphere lowered the reduction rate in the initial stages due to the poisoning effect of CO, but increased it in later stages due to the side reactions of the deposited carbon. Moon *et al.* (1998) also found a decrease in the reduction rate with CO content in the gas at 800–950 °C while reducing hematite compacts in H<sub>2</sub>-CO gas mixtures.

In the experiments of the thesis, the reduction potentials of H<sub>2</sub> and CO were set as equal by fixing the CO/CO<sub>2</sub> and H<sub>2</sub>/H<sub>2</sub>O ratios with respect to the CO<sub>2</sub> and H<sub>2</sub>O

formation reactions. The results show that the effect of adding 8% H<sub>2</sub>-H<sub>2</sub>O to the CO-CO<sub>2</sub> gas has an increasing effect on the rate of reduction of olivine pellets at temperatures of 750 and 800 °C, a slightly increasing effect at 850 °C and a negligible effect at 900, 1000 and 1150 °C. As for the reason for the higher reduction rate at lower temperatures, the WGSR must be considered, as it increases the amount of H<sub>2</sub> and thereby increases the reduction rate. At higher temperatures, where reverse WGSR is thermodynamically favourable, no significant differences in the reduction rates achieved by CO-CO<sub>2</sub> and H<sub>2</sub>-H<sub>2</sub>O-CO-CO<sub>2</sub> gas mixtures was detected, which indicates that an 8% H<sub>2</sub>-H<sub>2</sub>O addition does not affect reduction rate significantly at temperatures above 850 °C when reduction potentials of H<sub>2</sub> and CO are set as equal by fixing the CO/CO<sub>2</sub> and H<sub>2</sub>/H<sub>2</sub>O ratios.

The estimated activation energies for hematite to magnetite reduction indicated higher degree of reduction with H<sub>2</sub>-H<sub>2</sub>O-CO-CO<sub>2</sub> than with CO-CO<sub>2</sub> at 2% and 8% reduction. The better diffusivity of hydrogen to inner parts of the pellet can be considered as the reason for the higher reduction rate. Activation energies of reduction at 2% and 8% for the H<sub>2</sub>-H<sub>2</sub>O-CO-CO<sub>2</sub> mixture indicates a pore diffusion controlled mechanism and mixed control mechanism for the CO-CO<sub>2</sub> mixture, but ascertaining the rate controlling mechanism at the different reduction stages would need further investigation, such as processing the reduction data with developed mathematical equations for proposed reduction mechanisms and morphological observations (Sohn & Jung 2011). Larger wüstite relics were found in the inner parts of the pellet reduced to iron in CO-CO<sub>2</sub> but not in the pellet reduced in H<sub>2</sub>-H<sub>2</sub>O-CO-CO<sub>2</sub> at 1150 °C. Still, no significant difference was detected in the reduction rates of these gases at 1150 °C. According to Biswas (1981), H<sub>2</sub> is thermodynamically more efficient than CO for wüstite reduction at above 821 °C. The smaller molecule size of H<sub>2</sub> than CO provides more efficient diffusion to the inner parts of the pellet.

## **5.2 The WGSR and BF shaft conditions**

In the LF experiment of the thesis with hematite pellets, the WGSR was observed to occur simultaneously with the hematite to magnetite reduction at 400–450 °C. The LF experiment with pre-reduced magnetite pellets showed indications of the WGSR at 300–400 °C, pointing out the catalysing effect of magnetite. The equilibrium constants of the MPL experiment show the significant effect of the magnetite catalyst on the gas conversion. After the reduction of hematite to magnetite is complete, the H<sub>2</sub> formation rate settles on a steady level at 500 °C in

the HPL experiment. In the MPL experiment, the gas conversion rate settles on the same level at the same temperature. The highest WGSR reaction rates were detected in the lowest 5 cm layer of pellets in both HPL and MPL experiments. The rate of the WGSR dropped to practically zero in the 10–15 cm part of the pellet layer. This observation indicates that the gas converts almost totally to the thermodynamic equilibrium after flowing through the lowest 10 cm layer of magnetite pellets.

According to the results of this study, it is possible that the WGSR also takes place in the BF shaft when the water vapour concentration is high and magnetite is present. This situation can occur in the BF, when ascending gas contacts a magnetite layer in the upper shaft area. Due to lower temperature and weaker gas current near the walls of the shaft it is possible that moist material descend deeper in the shaft. Since the gas flow is stronger and the temperature is higher in the middle of the shaft than near the walls, it is possible that water evaporated near the walls gets swept away by the gas to the middle area of the shaft. Consequently, this can lead to the occurrence of the forward WGSR in a magnetite pellet layer. The suggested hypothesis for the WGSR in the BF shaft is illustrated in Fig. 39.

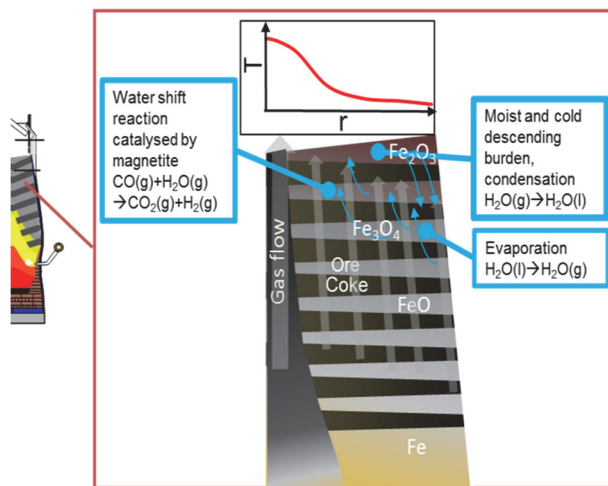


**Fig. 39. Illustration of the suggested hypothesis for the burden moisture behaviour near the wall in the upper part of the BF shaft and for the WGSR occurrence in the magnetite pellet layer (Paper II, reprinted by permission of ISIJ International).**

The more magnetite present in the range of 300 to 600 °C, the stronger the effect of the forward WGSR on the gas composition in the BF shaft can be considered to have. A study made by Ono-Nakazato *et al.* (2003) showed similar gas conversion transitioning towards equilibrium in experiments conducted on the reverse WGSR with CO-CO<sub>2</sub>-H<sub>2</sub>-H<sub>2</sub>O-N<sub>2</sub> gas at high temperatures in a packed bed.

Studies of dissected blast furnaces have shown that the distribution of the reduction degree varies between blast furnaces and is dependent on the operating conditions (Kanbara *et al.* 1977, Shimomura *et al.* 1977). High water vapour concentration in the upper BF shaft area can have an effect on the reduction reactions and the utilisation of the BF gas, since the H<sub>2</sub> and CO<sub>2</sub> concentrations increase and H<sub>2</sub>O and CO concentrations decrease through the WGSR, respectively. A study made by Nogami *et al.* (2012) on sinter reduction showed that a small addition of H<sub>2</sub> in the reducing gas increases the reduction rate of hematite but a further H<sub>2</sub> increase starts to decrease the reduction rate at 500 °C. An H<sub>2</sub> content higher than 2 vol-% in the CO-CO<sub>2</sub>-H<sub>2</sub>-H<sub>2</sub>O-N<sub>2</sub> gas does not seem to increase the reduction rate, but has a disadvantageous effect on the reduction rate, and the reduction degree obtained with 12 vol-% H<sub>2</sub> is the same as with 0 vol-% H<sub>2</sub>. However, when more H<sub>2</sub> is present in the reducing gas, the reduction-disintegration of the ore decreases improving the permeability of the burden, and this needs to be taken into consideration.

In the steel plant H<sub>2</sub> utilisation efficiency ( $\eta_{H_2}$ ) in the BF is determined by top gas analysis:  $\eta_{H_2} = H_2O / (H_2 + H_2O_{process})$ . Occurrence of the WGSR increases the amount of H<sub>2</sub> in the top gas which decreases  $\eta_{H_2}$  value. This causes error to the calculated  $\eta_{H_2}$ .

The gas conversion caused by the WGSR changes the heat value of the BF top gas, which is usually utilised in the pre-heating process of Cowper furnaces. From the viewpoint of the BF gas, the heat value of CO (CO + 1/2O<sub>2</sub> = CO<sub>2</sub>,  $\Delta H = -283.6$  kJ/mol at 200 °C) is higher compared to the one of H<sub>2</sub> (H<sub>2</sub> + 1/2O<sub>2</sub> = H<sub>2</sub>O,  $\Delta H = -243.5$  kJ/mol at 200 °C) which makes the occurrence of the WGSR unfavourable (Roine 2009). Also other reactions, such as the water gas reaction (C + H<sub>2</sub>O → CO + H<sub>2</sub>), can be expected to become more significant at high temperatures (>1000 °C), lower in the BF shaft, when H<sub>2</sub> and H<sub>2</sub>O concentrations are high. Since the reduction of iron oxide by H<sub>2</sub> is an endothermic reaction, this changes the temperature profile in the BF remarkably, which should also be considered.

The effect of high H<sub>2</sub> and H<sub>2</sub>O concentrations still requires further investigation in different parts of the BF shaft to obtain a better understanding of the phenomena occurring in the BF process.

Theoretically, the presence of the catalyst and a favourable temperature in the upper BF shaft area enable the progression of the forward WGSR. Although the gas approaches the equilibrium composition in the BF shaft through the WGSR, it is generally known that the BF top gas is not at thermodynamic equilibrium at the existing temperature when it exits the BF top. A typical BF top gas composition is in thermodynamic equilibrium at 600–800 °C temperature (Murakami *et al.* 2012).

### 5.3 High temperature properties of cold-bonded briquette

The reduction experiments which were conducted in the phase stability areas of magnetite and wüstite did not show significant difference between the reduction behaviour of the iron ore pellet and the briquette samples. However, a notable difference in the reduction behaviour of briquette samples and the pellet was detected between conducted in the phase stability area of iron. (“Iron 1” and “Iron 2”). The briquette reduced notably faster than the pellet in “Iron 1” experiment, which was an interrupted experiment up to 1100 °C. Thermodynamic computations were used in the present work to confirm complete reduction of briquette in (“Iron 1” and “Iron 2”) experiments. (Paper III).

The briquette samples contain about 10 wt-% carbonaceous material, mainly in the form of coke dust. It has been shown in the literature that at high temperatures (>800 °C), the high carbon gasification with CO<sub>2</sub> causes strong CO formation, which accelerates the reduction of the iron oxides considerably (Liu *et al.* 2004). The reduction of iron oxides in the direct reduction system is known to occur in gaseous phases (Fruehan 1977). In the case of coke dust, the gasification occurs at 750–850 °C in CO<sub>2</sub> gas, depending on the surrounding materials, which may act as catalysts (Hilding *et al.* 2005). The gasification temperature depends on the coke source. In the present study, coke dust showed no significant effect on temperatures below 780 °C in CO-CO<sub>2</sub>-N<sub>2</sub> gas, which is in agreement with the results of other authors (Fruehan 1977, Hilding *et al.* 2005, Liu *et al.* 2004).

In the literature, the self-reducing effect of the briquette achieved by carbon has been shown to lead to hematite to magnetite reduction at 500–600 °C, magnetite to wüstite at 640–850 °C and wüstite to iron at 850–1200 °C in an inert atmosphere. With sufficiently long heating time, a briquette has been shown to reach a 100% RD with the self-reduction in an inert atmosphere (Robinson 2005). In the present experiments, these reduction steps were reached in the briquette samples containing about 10 wt-% coke with interrupted reduction experiments, which simulated the BF conditions at 480, 780 and 1100 °C, respectively. The reference pellet did not

reach these reduction steps completely in the same experiments which can be explained by the direct reduction system achieved by the coke of the briquette. It is also possible that the self-reducing effect of the briquette may increase the reduction rate of the pellet due to coke gasification and increase of CO. It should be noticed that the reduction rate of the briquette is also increased by the higher porosity caused by the decomposition of the hydrates and the carbonates of the cement.

The self-reducing effect of the briquette was studied in the present experiments under simulated BF conditions and the briquettes can be predicted to have similar reduction behaviour in an actual BF. However, it must be noted that actual BF contains also H<sub>2</sub> and H<sub>2</sub>O gases and circulating elements such as potassium (K) and sulphur (S) which may have an effect on the coke gasification and the reduction reactions (Fruehan 1977, Hilding *et al.* 2005). The higher reduction rate of the briquettes compared to the pellets may need further consideration from the viewpoint of the briquettes' durability in the pressure of the BF shaft. The strength of the briquette samples were not tested after the experiments in this study.

According to the thesis results, the phase transformations and metamorphosis of the briquette samples follow the path of the compositions of the phase stability system of Fe-Fe<sub>2</sub>O<sub>3</sub>-CaO phase system in CO-CO<sub>2</sub>. The results show that briquettes reach the stable phase compositions in the interrupted reduction experiments.

In the present experiments, an increase of 25–50% in the volume of briquettes was detected during the wüstite-iron reduction step at 900–1000 °C. A 3% GGBFS addition showed an increasing effect on the swelling but a 6% GGBFS addition had no significant effect on the swelling. In the literature, the swelling of cold-bonded briquettes has been detected at the same temperature range and it has been explained to be caused by the popping up of individual pellet fines during the conversion of wüstite to iron (Singh & Björkman 2007a).

Singh & Björkman (2007a) have reported equal amount of swelling (approximately 31 vol-%) with cold-bonded briquettes under quite similar reduction conditions. They conducted the laboratory experiments under simulated BF conditions in N<sub>2</sub>-CO-CO<sub>2</sub>-H<sub>2</sub> gas at 10 l/min flow rate. They also found that in an experimental BF, the amount of swelling was at lower level (<15 vol-%).

Singh & Björkman (2007) detected catastrophic swelling (>100 vol-%) of cold-bonded briquettes in the experiments which were conducted under isothermal conditions at 950 °C using N<sub>2</sub> + CO (60:40). They suspected that the catastrophic swelling takes place in three steps: disintegration of pellet fines particles, formation of slag with low melting point and generation of localised high gas pressure owing

to formation and oxidation of metastable iron carbide ( $\text{Fe}_3\text{C}$ ). Formation reaction of  $\text{Fe}_3\text{C}$  is shown in Eq. 21.



The  $\text{Fe}_3\text{C}$  phase was not identified in the XRD analyses of this study, which explains the lack of catastrophic swelling due to formation of metastable iron carbide. The cause of catastrophic swelling in iron ore pellets is known to be due to growth of iron whiskers in wüstite reduction. The growth of iron whiskers has been shown to increase under certain conditions and in the presence of CaO (Nicolle & Rist 1979). The mechanism of whisker growth should also be considered for the cause of swelling of the briquettes in the present experiments because they consist of these raw materials. The GGBFS addition in the briquette basically increases the amount of CaO and decreases the amount of iron oxides which might have an effect on the swelling behaviour.

#### **5.4 Softening mechanism of the iron ore pellet**

The results of the softening experiments presented in this work showed different softening behaviour for iron ore pellets with markedly different chemistry under inert conditions. The acid pellet softened rapidly at 1150 °C and reached approximately 40% contraction at 1200 °C. Rapid softening and significant gas pressure losses has been detected at around 1150 °C in the industrial reduction-softening (ARUL equipment with MASSIM programme) packed bed test conducted on similar acid pellets (Iljana *et al.* 2015b). Comparison of these results indicates of early deformation of the acid pellet which leads to a pressure loss in a packed bed test. According to the results of this work the olivine fluxed pellet softened gradually from 1150 °C and reached approximately 30% contraction at 1350 °C. Similar softening behaviour was detected in the ARUL packed bed test conducted on similar olivine fluxed pellets (Iljana *et al.* 2015a).

No significant differences were detected in the softening properties within acid pellets pre-reduced to 50–70% or within olivine fluxed pellets pre-reduced to 50–65% under BF simulation conditions. It was seen that a pellet pre-reduced up to 1100 °C consists of a porous metallic iron shell and an oxide core. The thickness of the metallic iron shell and the phase composition of the oxide core are determined by the RD and the chemistry of the pellet, respectively. It must be noted that in this case the pellets were reduced by the BFS under no load which might have an effect on the structure of the metallic iron shell. In the actual BF,  $\text{H}_2$  is also

present in the reducing gas which probably affects the structure formation in during reduction.

The pellet with the lowest RD reached the highest contraction-% at maximum temperatures in both cases. A visual observation made by LOM showed that the metallic iron shells of the pre-reduced pellets consist of a layer of separate particles. The pellets with higher RD have a higher metallic iron content and lower divalent iron content. The results indicate that the thicker metallic iron layer does not increase the softening temperature of the pellet markedly.

The highest contraction-% of pellets with the lowest RD could be explained by having a larger deformable oxide core. Since the conditions in the present experiments differ from the softening and melting experiments made by other authors, the results are not fully comparable. Some similarities can still be found in the softening temperatures. In the study conducted by Nogueira *et al.* (2004), slight differences in the softening behaviour of iron ore pellets with RDs of 60–80% were detected. Their study showed similar contraction of the pellets with high SiO<sub>2</sub> content (3–5 wt-%) as shown in this study with the acid pellets (5.27 wt-% SiO<sub>2</sub>).

The results of this study suggest that the oxide core of the pellet plays an important role in softening behaviour. The FESEM-EDS analyses showed that the core part of the softened pellet consists mainly of wüstite and fayalite slag phase. The fayalite slag phase of the acid pellet has approximately 0.5–2 wt-% CaO and 0.5–1.5 wt-% MgO as dissolved components and the slag phase of the olivine fluxed pellet has 4 wt-% MgO and 5 wt-% CaO, respectively. Additionally, the wüstite phase in the olivine fluxed pellet has about 1 wt-% dissolved MgO.

The results indicate superior high-temperature properties of the olivine fluxed pellet and inferior properties of the acid pellet. Similar behaviour was seen in previous studies also with acid and olivine fluxed pellet. They attributed the superior properties of the olivine pellet to high reducibility and high MgO which increases the melting temperature of the slag and the wüstite. The inferior properties of acid pellet were caused by the early softening. They also studied the softening and melting properties of lime (CaO) fluxed pellets which showed high reducibility and increased meltdown temperatures due to the high melting-point slag phase. The good high temperature properties of the lime fluxed pellet were attributed to excellent reducibility and low SiO<sub>2</sub> content. The acid pellet had the lowest 50% shrinkage temperature and the lime fluxed pellet had the highest. (Borinder & Yang 1987, Borinder & Bi 1989).

Quaternary FeO-SiO<sub>2</sub>-CaO-MgO-systems with constant contents of CaO and MgO which were computed using FactSage V6.4 -software and its FToxid-database

was found to be a useful tool to in testing the effect of fluxes on the solidus and liquidus temperatures of the FeO-SiO<sub>2</sub> phase systems which are commonly present in iron ore pellets. A liquid oxide phase evolution as a function of temperature was also computed by FactSage (Bale *et al.* 2013). Thermodynamic calculations show that the amounts of SiO<sub>2</sub> and fluxes (CaO, MgO) have a significant role in the softening properties of pellet. The higher SiO<sub>2</sub> content will form higher amount of slag and therefore higher dissolution of the wüstite in it. The dissolution and separation of the wüstite phase into single particles appears to cause the deformation of the structure under pressure. In the case of the acid pellet, reaching the solidus temperature of the slag launches the early softening. The superior softening properties of the olivine fluxed pellet can be attributed to the low SiO<sub>2</sub> content and higher amount of fluxes since less slag is formed and the preventive effect of the fluxes (MgO) on the wüstite dissolution. However, the large number of different components and reactions between them needs further testing to clarify the phenomena between the SiO<sub>2</sub> and the fluxes.

It should be noticed that increasing the amount of fluxes also increases the melting temperature of wüstite. In order to optimise the quantity of fluxes the effect of SiO<sub>2</sub> content needs further testing, because the computed phase systems cannot predict the softening caused by the wüstite dissolution. E.g. the FactSage computed FeO-SiO<sub>2</sub>-CaO-MgO diagram in Fig. 34 shows that decreasing the amount of SiO<sub>2</sub> in the acid pellet by 2–3 wt-% will actually decrease the solidus temperature of the system, which is an unfavourable effect. However, the amount of the slag phase is also reduced, which is supposed to have an enhancing effect on the softening properties since the dissolution of the wüstite is reduced. Clarification of this effect needs further testing. From the viewpoint of early softening, the optimum composition is probably found by adjusting the quantity of SiO<sub>2</sub> and fluxes. A reasonable correlation was found between the computed liquid slag fraction-% and the pellet contraction-% observed in the experiments. This indicates that the share of the liquid slag in the pellet has an important role in the softening behaviour. The quantity of SiO<sub>2</sub> and fluxes has an effect on the evolution of liquid slag phase in the iron ore pellet.

## 5.5 Industrial relevance of the thesis

In order to reduce the consumption of metallurgical coke in steel plants, increasing amounts of injected reductants are being used as a coke replacement in the BF. The high rate of injected reductants increases the concentrations of H<sub>2</sub> and H<sub>2</sub>O in the

BF shaft which has an effect on the iron oxide reduction reactions. The effect of high injection on the iron oxide reduction reactions in the BF shaft is not fully known. This thesis provides additional information about the effect of H<sub>2</sub> on the iron oxide reduction reactions. (Paper I).

At SSAB Europe Raahe steelworks in Finland, the BF charging procedure of iron oxides has been recently changed from mixed sinter and pellet to mixed pellet and cold-bonded briquette. This change requires a lot of laboratory and pilot scale tests because the amount of the charged pellets being used has increased considerably and the cold-bonded briquettes are a totally new raw material.

The charged pellets are water-treated to prevent dust emissions and, in addition, they contain varying degrees of moisture as they have been stored outdoors. The cold-bonded briquettes contain approximately 10% water which reacts with the binder to form a sufficiently strong structure. This chemically bound water is released in the BF shaft in hydrate decomposition reactions. At the time of mixed sinter and pellet charging, the burden moisture content was at a negligible level, because the pellets were stored indoors and sinters were provided by a sinter plant situated at the steelworks in Raahe. With the current BF charging procedure, there has been detected notable change in the temperature profile of the upper part of the BF shaft and in the values of  $\eta_{CO}$  and  $\eta_{H_2}$ . These observations indicate that it is possible that moist burden descends deeper in the shaft near the BF walls than in the middle part, before all moisture evaporates due to lower temperature and weaker gas current. Since the gas flow is stronger and the temperature is higher in the middle of the shaft than near the walls, it is possible that water evaporated near the walls gets swept away by the gas to the middle area of the shaft. Consequently, this can lead to the occurrence of the forward WGSR in a magnetite pellet layer. This thesis provides information about the effect of the high water vapour concentration on the gas phase reactions through the magnetite catalysed WGSR in the upper part of the BF shaft. (Paper II).

The chemistry of the cold-bonded briquette differs considerably from the pellet and therefore the high temperature properties have to be tested before charging it in the BF process. The cold-bonded briquette contains decomposing components which require additional energy for breaking the bonds. It also contains embedded carbon which causes the self-reducing effect. The reduction behaviour of the cold-bonded briquette was studied in this thesis under reducing conditions which simulated the indirect reduction zone of the BF. (Paper III).

Since the amount of charged pellets is increased markedly, the formation of the cohesive zone is mainly determined by the softening and melting properties of the

iron ore pellets. The location and shape of the cohesive zone has a significant effect on the BF efficiency. In this work, the softening behaviour of the acid and olivine fluxed iron ore pellets are experimentally tested. This thesis clarifies the fundamentals of the iron ore pellet softening and suggests computed phase evolution as a tool to predict and study further the softening behaviour of an iron ore pellet. (Paper IV).



## 6 Conclusions

The most important conclusions reached among the topics of this thesis can be summarised as follows:

The effect of H<sub>2</sub> on the reduction of iron oxides:

- 8% H<sub>2</sub>-H<sub>2</sub>O addition to the CO-CO<sub>2</sub> gas had an increasing effect on the rate of reduction of olivine pellets at temperatures 750 and 800 °C and slightly increasing effect at 850 °C. At temperatures of 900, 1000 and 1150 °C no significant influence on the reduction rate was detected by replacing 8% of the CO-CO<sub>2</sub> mixture with an H<sub>2</sub>-H<sub>2</sub>O mixture at a ratio where the equilibrium partial pressures of oxygen for the carbon dioxide and water vapour formation reactions were equal.
- The accelerating influence of hydrogen shown in the literature with pure reductive gases was detected at temperatures 750–850 °C but not at temperatures above 900 °C with H<sub>2</sub>-H<sub>2</sub>O-CO-CO<sub>2</sub> mixtures.
- The activation energies determined for hematite to magnetite reductions and indicated higher degree of reduction with the H<sub>2</sub>-H<sub>2</sub>O-CO-CO<sub>2</sub> gas than with CO-CO<sub>2</sub> at 2% and 8% reduction.
- Scanning electron microscope analysis pointed to wüstite relics in the inner parts of the pellet reduced to iron in CO-CO<sub>2</sub> atmosphere which indicates better wüstite reduction with the H<sub>2</sub>-H<sub>2</sub>O-CO-CO<sub>2</sub> gas than with CO-CO<sub>2</sub>.

The effect of the high water vapour concentration in the upper Blast Furnace (BF) shaft:

- The Water-Gas Shift Reaction (WGSR) was observed in the hematite pellet layer simultaneously with the hematite to magnetite reduction step at 400–450 °C, indicating the catalysing effect of the magnetite formed in the reduction reaction.
- In the pre-reduced magnetite pellet layer the WGSR was observed at above 300 °C and the gas converted rapidly to the thermodynamic equilibrium through the WGSR. Equilibrium gas composition was reached after 15 cm layer of pellets in the layer furnace.
- With high water vapour concentration, the WGSR can alter the reducing gas composition in the BF shaft when the ascending gas confronts a magnetite layer and thus affects the reduction reactions and the utilisation of the BF top

gas. From the perspective of BF gas utilisation, the occurrence of the WGSR is unfavourable when the heat values of CO and H<sub>2</sub> are compared.

The reduction behaviour cold-bonded by-product briquettes:

- The briquettes showed significantly faster reduction compared to an iron ore pellet when reduced to metallic iron at 780–1100 °C temperature due to the self-reduction effect achieved by the coke.
- An increase of 25–50% in the volume of briquettes was detected during the wüstite-iron reduction step at 900–1000 °C.
- Phase transformations occurring in the briquette are in agreement with the theory and briquettes can be predicted to follow the phase transformation path in the actual BF process.
- The structure of the briquette does not disintegrate in the BF conditions even though the cement phases decompose in the high temperature of the BF process. The phase transformation of Ca(OH)<sub>2</sub> first to CaCO<sub>3</sub> and secondly to Ca<sub>2</sub>Fe<sub>2</sub>O<sub>5</sub> may have an effect on this behaviour.

Softening behaviour of iron ore pellets in the cohesive zone of the BF:

- The acid pellet softened rapidly at 1150 °C and reached about 40% contraction at 1200 °C. The olivine fluxed pellet began to soften gradually at 1150 °C and reached contraction 30–35% at 1350 °C.
- The phase composition of the oxide core has a significant role in the softening properties since the softening is caused by the wüstite dissolution in the slag phase.
- The high amount of the SiO<sub>2</sub> leads to early softening caused by the high dissolution of wüstite in the slag phase which separates the wüstite phase into separate particles.
- Early softening caused by the dissolution of wüstite could be avoided by decreasing the quantity of SiO<sub>2</sub> and adding fluxes (CaO, MgO) in appropriate amounts.

## 7 Recommendations for future work

The study performed on the effect of  $H_2$  on the iron oxide reduction and the activation energies at 2% and 8% of reduction as well as indicating the pore diffusion mechanism for a  $H_2$ - $H_2O$ - $CO$ - $CO_2$  mixture and mixed control mechanism for a  $CO$ - $CO_2$  mixture. However, the determination of the rate controlling mechanism at the different reduction stages would need further investigation, such as processing the reduction data with developed mathematical equations for proposed reduction mechanisms and morphological observations. In this thesis, the determination of rate controlling mechanism was not made on these mixtures and therefore it is recommended as an area for future work.

Considerations about the effect of the WGSR in upper part of the BF shaft revealed that evaporation of moisture and condensation of water vapour are complex processes and the determination of the critical temperatures for these phenomena to occur in a moist gas flow needs further investigation.

The self-reduction showed a significant effect on the reduction behaviour of the cold-bonded briquette in the simulated BF shaft conditions when compared to the iron ore pellet. The briquettes are in contact with the pellets in the actual BF and therefore they may have an effect on the pellet reduction. A mixed burden reduction test is recommended for future work to investigate the effect of the self-reduction of the briquette on the reduction of iron ore pellet.

The superior high temperature properties of the olivine fluxed pellet and inferior properties of the acid pellet indicate that the amounts of  $SiO_2$  and fluxes ( $CaO$ ,  $MgO$ ) have a significant role in the softening properties of pellet. The higher  $SiO_2$  content will form a higher amount of slag and therefore a higher dissolution of the wüstite in it, which eventually collapses the uniform structure. However, the large number of different components and reactions between them needs further testing to clarify the phenomena between the  $SiO_2$  and the fluxes. The thermodynamic calculations of this work proved to be a useful tool in testing the effect of fluxes on the solidus and liquidus temperatures of the  $FeO$ - $SiO_2$  phase systems which are commonly present in iron ore pellets. In order to optimise the quantity of fluxes, the effect of  $SiO_2$  content needs further testing, because the computed phase systems cannot predict the softening caused by the wüstite dissolution.



## References

- Alatarvas T, Iljana M, Mattila O, Paananen T & Fabritius T (2012) Scanmet IV, 4th Int. Conf. on Process Development in Iron and Steelmaking 1: 385.
- Atlas S (1995) Verein Deutscher Eisenhüttenleute.
- Babich A, Senk D, Gudenau HW & Mavrommatis K (2008) Ironmaking. Aachen, Germany, RWTH Aachen University.
- Bakker T (1999) Softening in the Blast Furnace: Local Melt formation as the Trigger for Softening of Ironbearing Burden Materials. Ph.D thesis. Delft, The Netherlands, Delft University of Technology.
- Bale CW, Pelton AD, Thompson WT, Eriksson G, Hack K, Chartrand P, Decterov S, Jung I-H, Melancon J & Petersen S (2013) FactSage, V6.4, Software and Its Database.
- Barnaba P (1985) Influence of chemical characteristics on softening and melting-down properties of iron ore sinter. *Ironmaking and Steelmaking* 12(2): 53–63.
- Beppler E, Kannappel M, Kowalski W, Langner K, Müllheims K & Wachsmuth H (1998) ECSC Workshop: 111.
- Biswas AK (1981) Principles of Blast Furnace Ironmaking: Theory and practice. Brisbane, Cootha Publishing House.
- Borinder T & Bi X (1989) Softening-Melting Properties of Pellets Under Simulated Blast Furnace Conditions. *Scand J Metall* 18(6): 280–287.
- Borinder T & Yang Z (1987) High Temperature Behaviour of Some Blast Furnace Pellets. II. *Scand J Metall* 16(3): 129–133.
- Chidiac SE & Panesar DK (2008) Evolution of mechanical properties of concrete containing ground granulated blast furnace slag and effects on the scaling resistance test at 28 days. *Cement and Concrete Composites* 30(2): 63–71.
- El-Geassy AA (1986) Gaseous reduction of Fe<sub>2</sub>O<sub>3</sub> compacts at 600 to 1050 °C. *J Mater Sci* 21(11): 3889–3900.
- El-Geassy AA, Shehata KA & Ezz SY (1977) Mechanism of iron oxide reduction with hydrogen/carbon monoxide mixtures. *Trans Iron Steel Inst Jpn* 17(11): 629–635.
- Escalante JI, Gómez LY, Johal KK, Mendoza G, Mancha H & Méndez J (2001) Reactivity of blast-furnace slag in Portland cement blends hydrated under different conditions. *Cem Concr Res* 31(10): 1403–1409.
- Fruehan RJ (1977) Rate of reduction of iron oxides by carbon. *Metall Trans B* 8 B(2): 279–286.
- Geerdes M, Toxopeus H & van der Vliet C (2009) Modern Blast Furnace Ironmaking. Amsterdam, The Netherlands, IOS Press BV.
- Gudenau HW, Stoesser K, Denecke H & Schemmann V (2000) Environmental aspects and recycling of filter dusts by direct injection or use of agglomerates in shaft furnaces. *ISIJ Int* 40(3): 218–223.
- Hilding T, Gupta S, Sahajwalla V, Björkman B & Wikström J-O (2005) Degradation behaviour of a high CSR coke in an Experimental Blast Furnace: Effect of carbon structure and alkali reactions. *ISIJ Int* 45(7): 1041–1050.

- Iljana M, Kemppainen A, Heikkinen E-P, Paananen T, Mattila O & Fabritius T (2015) A new sophisticated method for evaluating the reduction-softening properties of iron burden materials. METEC & 2nd ESTAD, European Steel Technology and Application Days. Düsseldorf, Germany, Steel Institute VDEh.
- Iljana M, Kemppainen A, Paananen T, Pisilä E, Kondrakov M & Fabritius T (2015) Effect of Limestone Addition on the Metallurgical Properties of Iron Ore Pellet. *International journal of mineral processing* 141: 34.
- Iljana M, Mattila O, Alatarvas T, Kurikkala J, Paananen T & Fabritius T (2013) Effect of circulating elements on the dynamic reduction swelling behaviour of olivine and acid iron ore pellets under simulated blast furnace shaft conditions. *ISIJ Int* 53(3): 419–426.
- Iljana M, Mattila O, Alatarvas T, Visuri VV, Kurikkala J, Paananen T & Fabritius T (2012) Dynamic and isothermal reduction swelling behaviour of olivine and acid iron ore pellets under simulated blast furnace shaft conditions. *ISIJ Int* 52(7): 1257–1265.
- ISO 13930:2007: Iron ores for blast furnace feedstocks - Determination of low-temperature reduction-disintegration indices by dynamic method, 9, International Organization for Standardization, Geneva, 2007.
- ISO 4698:2007: Iron ore pellets for blast furnace feedstocks - Determination of the free-swelling index. International Organization for Standardization, Geneva, 2007.
- ISO 7215:2007: Iron ores for blast furnace feedstocks - Determination of the reducibility by the final degree of reduction index. International Organization for Standardization, Geneva, 2007.
- ISO 7992:2007: Iron ores for blast furnace feedstocks - Determination of reduction under load. International Organization for Standardization, Geneva, 2007.
- Kanbara K, Hagiwara T, Shigemi A, Kondo S, Kanayama Y, Wakabayashi K & Hiramoro N (1977) *Trans. Iron Steel Inst. Jpn.* 17: 372.
- Kasai A & Matsui Y (2004) Lowering of thermal reserve zone temperature in blast furnace by adjoining carbonaceous material and iron ore. *ISIJ Int* 44(12): 2073–2078.
- Kaushik P & Fruehan RJ (2006) Mixed burden softening and melting phenomena in blast furnace operation Part 1 - X-ray observation of ferrous burden. *Ironmaking and Steelmaking* 33(6): 507–519.
- Kaushik P & Fruehan RJ (2006) Mixed burden softening and melting phenomena in blast furnace operation Part 2 - Mechanism of softening and melting and impact on cohesive zone. *Ironmaking and Steelmaking* 33(6): 520–528.
- Kemppainen A, Iljana M, Heikkinen E-P, Paananen T, Mattila O & Fabritius T (2014) Reduction behavior of cold-bonded briquettes under simulated blast furnace conditions. *ISIJ Int* 54(7): 1539–1545.
- Kemppainen A, Mattila O, Heikkinen E-P, Paananen T & Fabritius T (2012) Effect of H<sub>2</sub>-H<sub>2</sub>O on the reduction of olivine pellets in CO-CO<sub>2</sub> gas. *ISIJ Int* 52(11): 1973–1978.
- Ke-qin M & Jia-xin L (1993) Changes of Burden Behaviour in BF with Oxygen-Coal Injection. *Journal of East China Institute of Metallurgy*, 1993, 10 (4): 1–6 (in Chinese).
- Kowitwarangkul P, Babich A & Senk D (2014) Reduction behavior of self-reducing pellet (SRP) for low height blast furnace. *Steel Research International* 85(11): 1501–1509.

- Li J, Wang P, Zhou L & Cheng M (2007) The reduction of wüstite with high oxygen enrichment and high injection of hydrogenous fuel. *ISIJ Int* 47(8): 1097–1101.
- Liu G-S, Strezov V, Lucas JA & Wibberley LJ (2004) Thermal investigations of direct iron ore reduction with coal. *Thermochimica Acta* 410(1–2): 133–140.
- Mäkelä M, Paananen T, Heino J, Kokkonen T, Huttunen S, Makkonen H & Dahl O (2012) Influence of fly ash and ground granulated blast furnace slag on the mechanical properties and reduction behavior of cold-agglomerated blast furnace briquettes. *ISIJ Int* 52(6): 1101–1108.
- Martos C, Dufour J & Ruiz A (2009) Synthesis of Fe<sub>3</sub>O<sub>4</sub>-based catalysts for the high-temperature water gas shift reaction. *Int J Hydrogen Energy* 34(10): 4475–4481.
- Mondal K, Lorethova H, Hippo E, Wiltowski T & Lalvani SB (2004) Reduction of iron oxide in carbon monoxide atmosphere - Reaction controlled kinetics. *Fuel Process Technol* 86(1): 33–47.
- Moon I-J, Rhee C-H & Min D-J (1998) Reduction of hematite compacts by H<sub>2</sub>-CO gas mixtures. *Steel Res* 69(8): 302–306.
- Murakami T, Kamiya Y, Kodaira T & Kasai E (2012) Reduction disintegration behavior of iron ore sinter under high H<sub>2</sub> and H<sub>2</sub>O conditions. *ISIJ Int* 52(8): 1447–1453.
- Nakano M, Naito M, Higuchi K & Morimoto K (2004) Non-spherical carbon composite agglomerates: Lab-scale manufacture and quality assessment. *ISIJ Int* 44(12): 2079–2085.
- Newsome DS (1980) Water-gas shift reaction. *Catalysis reviews Softcover ed.* 21(2): 275–281.
- Nicolle R & Rist A (1979) The mechanism of whisker growth in the reduction of wüstite. *Metallurgical Transactions B* 10(3): 429–438.
- Nogami H, Kashiwaya Y & Yamada D (2012) Simulation of blast furnace operation with intensive hydrogen injection. *ISIJ Int* 52(8): 1523–1527.
- Nogueira PF & Fruehan RJ (2004) Blast furnace burden softening and melting phenomena: Part I. Pellet bulk interaction Observation. *Metall Mat Trans B Process Metall Mat Process Sci* 35(5): 829–838.
- Nogueira PF & Fruehan RJ (2005) Blast furnace burden softening and melting phenomena: Part II. Evolution of the structure of the pellets. *Metall Mat Trans B Process Metall Mat Process Sci* 36(5): 583–590.
- Nogueira PF & Fruehan RJ (2006) Blast furnace burden softening and melting phenomena: Part III. Melt onset and initial microstructural transformations in pellets. *Metall Mat Trans B Process Metall Mat Process Sci* 37(4): 551–558.
- Oeters F, Ottow M, Senk D, Beyzavi A, Güntner J, Lungen HB, Koltermann M & Buhr A (2011) *Ullman's Encyclopedia of Industrial Chemistry* 19: 577.
- Ono-Nakazato H, Yonezawa T & Usui T (2003) Effect of Water-Gas Shift Reaction on Reduction of Iron Oxide Powder Packed Bed with H<sub>2</sub>-CO Mixtures. *ISIJ Int* 43(10): 1502–1511.
- Osborne GJ (1999) Durability of Portland blast-furnace slag cement concrete. *Cement and Concrete Composites* 21(1): 11–21.

- Paananen T (2013) The Effect of Minor Oxide Components on Reduction of Iron Ore Agglomerates. Doctoral thesis. Oulu, University of Oulu.
- Peters K-H, Beppler E, Gerstenberg B & Janhsen U (1994) 53rd Ironmaking Conf. Proc., Iron and Steel Society, Warrendale, PA: 257.
- Piotrowski K, Mondal K, Lorethova H, Stonawski L, Szymański T & Wiltowski T (2005) Effect of gas composition on the kinetics of iron oxide reduction in a hydrogen production process. *Int J Hydrogen Energy* 30(15): 1543–1554.
- Rhodes C, Hutchings GJ & Ward AM (1995) Water-gas shift reaction: finding the mechanistic boundary. *Catalysis Today* 23(1): 43–58.
- Ritz V, Mülheims K, Rosenplänter R, Lectard E & Bürgler T (2004) Critical Review of Existing Procedures for the Characterisation of the Metallurgical Properties of Blast Furnace Burden Material at Conditions of High Injections Rates: 153.
- Robinson R (2005) High temperature properties of by-product cold bonded pellets containing blast furnace flue dust. *Thermochimica Acta* 432(1): 112–123.
- Robinson R, Patisson F & Björkman B (2011) Low temperature reactivity in agglomerates containing iron oxide: Studies in the Ca(OH)<sub>2</sub>-C-Fe<sub>2</sub>O<sub>3</sub> system. *Journal of Thermal Analysis and Calorimetry* 103(1): 185–193.
- Roine A (2009) Outotec HSC Chemistry Ver.7.00 for Windows, Outotec Research Oy, Pori, Finland.
- Sastri MVC, Viswanath RP & Viswanathan B (1982) Studies on the reduction of iron oxide with hydrogen. *Int J Hydrogen Energy* 7(12): 951–955.
- Satterfield CN (1991) *Heterogeneous Catalysis in Industrial Practice*.
- Schuermann E & Wurm P (1973) Phase Diagrams and Reduction Equilibria of the Ternary System Fe-Fe<sub>2</sub>O<sub>3</sub>-CaO Between 550 and 1071 degree C. *Arch Eisenhuettenwes* 44(9): 637–645.
- Shimomura Y, Nishikawa K, Arino S, Katayama T, Hida Y & Isoyama T (1977) On the internal state of the lumpy zone of blast furnace. *Trans. ISIJ* 17: 381–390.
- Singh M & Björkman B (2004) Effect of processing parameters on the swelling behaviour of cement-bonded briquettes. *ISIJ Int* 44(1): 59–68.
- Singh M & Björkman B (2006) Strength of cement-bonded briquettes. *Minerals and Metallurgical Processing* 23(4): 203–213.
- Singh M & Björkman B (2007) Testing of cement bonded briquettes under laboratory and blast furnace conditions Part 1 - Effect of processing parameters. *Ironmaking and Steelmaking* 34(1): 30–40.
- Singh M & Björkman B (2007) Testing of cement bonded briquettes under laboratory and blast furnace conditions Part 2 - Swelling of briquettes. *Ironmaking and Steelmaking* 34(1): 41–53.
- Smith B, Loganathan RJM & Shantha MS (2010) *Int. J. Chem. Reactor Eng.* 8.
- Sohn I & Jung SM (2011) Effect of Metal Additions to the Reduction of Iron Oxide Composite Pellets with Hydrogen at Moderate Temperatures. *Steel research international* 82(12): 1345–1354.

- Sterneland J, Andersson MAT & Jönsson PG (2003) Comparison of iron ore reduction in experimental blast furnace and laboratory scale simulation of blast furnace process. *Ironmaking and Steelmaking* 30(4): 313–327.
- Teräskirja 2014. Bookwell Oy, Metallinjalostajat ry.
- Towhidi N & Szekely J (1981) Reduction kinetics of commercial low-silica hematite pellets with CO-H<sub>2</sub> mixtures over temperature range 600 degree –1234 degree C. *Ironmaking and Steelmaking* 8(6): 237–249.
- Turkdogan ET & Vinters JV (1972) Gaseous reduction of iron oxides – 3. *Metall Trans* 3(6): 1561–1574.
- Usui T, Kawabata H, Ono-Nakazato H & Kurosaka A (2002) Fundamental experiments on the H<sub>2</sub> gas injection into the lower part of a blast furnace shaft. *ISIJ Int* 42(Suppl.): S14–S18.
- Walker RD (1986) *Modern Ironmaking Methods*. London, England, The Chameleon Press Ltd.



## Original publications

- I Kemppainen A, Mattila O, Heikkinen E-P, Paananen T & Fabritius T (2012) Effect of H<sub>2</sub>-H<sub>2</sub>O on the reduction of olivine pellets in CO-CO<sub>2</sub> gas. *ISIJ Int* 52(11): 1973–1978.
- II Kemppainen A, Alatarvas T, Iljana M, Haapakangas J, Mattila O, Paananen T & Fabritius T (2014) Water-gas shift reaction in an olivine pellet layer in the upper part of blast furnace shaft. *ISIJ Int* 54(4): 801–809.
- III Kemppainen A, Iljana M, Heikkinen E-P, Paananen T, Mattila O & Fabritius T (2014) Reduction behavior of cold-bonded briquettes under simulated blast furnace conditions. *ISIJ Int* 54(7): 1539–1545.
- IV Kemppainen A, Ohno K-I, Iljana M, Mattila O, Paananen T, Heikkinen E-P, Maeda T, Kunitomo K & Fabritius T (2015) Softening behaviors of acid and olivine fluxed iron ore pellets in the cohesive zone of a blast furnace. *ISIJ Int*. DOI: 10.2355/isijinternational.ISIJINT-2015-023.

Reprinted with permission from ISIJ International (I–IV).

Original publications are not included in the electronic version of the dissertation.



530. Leppänen, Kimmo (2015) Sample preparation method and synchronized thermography to characterize uniformity of conductive thin films
531. Pouke, Matti (2015) Augmented virtuality : transforming real human activity into virtual environments
532. Leinonen, Mikko (2015) Finite element method and equivalent circuit based design of piezoelectric actuators and energy harvester dynamics
533. Leppäjärvi, Tiina (2015) Pervaporation of alcohol/water mixtures using ultra-thin zeolite membranes : membrane performance and modeling
534. Lin, Jih-Fong (2015) Multi-dimensional carbonaceous composites for electrode applications
535. Goncalves, Jorge (2015) Situated crowdsourcing : feasibility, performance and behaviours
536. Herrera Castro, Daniel (2015) From images to point clouds : practical considerations for three-dimensional computer vision
537. Komulainen, Jukka (2015) Software-based countermeasures to 2D facial spoofing attacks
538. Pedone, Matteo (2015) Algebraic methods for constructing blur-invariant operators and their applications
539. Karhu, Mirjam (2015) Treatment and characterisation of oily wastewaters
540. Panula-Perälä, Johanna (2015) Development and application of enzymatic substrate feeding strategies for small-scale microbial cultivations : applied for *Escherichia coli*, *Pichia pastoris*, and *Lactobacillus salivarius* cultivations
541. Pennanen, Harri (2015) Coordinated beamforming in cellular and cognitive radio networks
542. Ferreira, Eija (2015) Model selection in time series machine learning applications
543. Lamminpää, Kaisa (2015) Formic acid catalysed xylose dehydration into furfural
544. Visanko, Miikka (2015) Functionalized nanocelluloses and their use in barrier and membrane thin films
545. Gilman, Ekaterina (2015) Exploring the use of rule-based reasoning in ubiquitous computing applications
546. Kempainen, Antti (2015) Limiting phenomena related to the use of iron ore pellets in a blast furnace

Book orders:

Granum: Virtual book store

<http://granum.uta.fi/granum/>

S E R I E S E D I T O R S

**A**  
**SCIENTIAE RERUM NATURALIUM**

*Professor Esa Hohtola*

**B**  
**HUMANIORA**

*University Lecturer Santeri Palviainen*

**C**  
**TECHNICA**

*Postdoctoral research fellow Sanna Taskila*

**D**  
**MEDICA**

*Professor Olli Vuolteenaho*

**E**  
**SCIENTIAE RERUM SOCIALIUM**

*University Lecturer Veli-Matti Ulvinen*

**E**  
**SCRIPTA ACADEMICA**

*Director Sinikka Eskelinen*

**G**  
**OECONOMICA**

*Professor Jari Juga*

**H**  
**ARCHITECTONICA**

*University Lecturer Anu Soikkeli*

**EDITOR IN CHIEF**

*Professor Olli Vuolteenaho*

**PUBLICATIONS EDITOR**

*Publications Editor Kirsti Nurkkala*

